CHALMERS

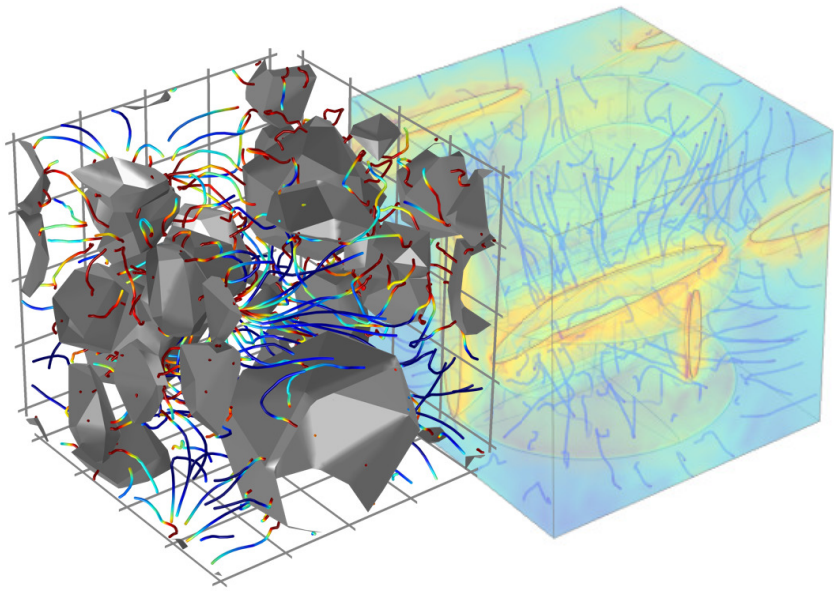

Multi-scale modeling and finite element simulation of diffusion in porous media

NELE POLLMANN

Department of Industrial and Materials Science
CHALMERS UNIVERSITY OF TECHNOLOGY
Göteborg, Sweden 2019

THESIS FOR THE DEGREE OF DOCTOR OF PHILOSOPHY IN SOLID AND STRUCTURAL MECHANICS

Multi-scale modeling and finite element simulation of diffusion in porous media

NELE POLLMANN

Department of Industrial and Materials Science
CHALMERS UNIVERSITY OF TECHNOLOGY

Göteborg, Sweden 2019

Multi-scale modeling and finite element simulation of diffusion in porous media
NELE POLLMANN
ISBN 978-91-7905-170-9

Doktorsavhandlingar vid Chalmers tekniska högskola
Ny serie nr. 4637
ISSN 0346-718X
Department of Industrial and Materials Science
Chalmers University of Technology
SE-412 96 Göteborg
Sweden
Telephone: +46 (0)31-772 1000

Cover:
Streamlines of mass flux in three phase concrete with 40% aggregate volume fraction (left). Streamlines and pore pressure amplitudes in fractured poroelastic rock.

Chalmers Reproservice
Göteborg, Sweden 2019

Multi-scale modeling and finite element simulation of diffusion in porous media
NELE POLLMANN
Department of Industrial and Materials Science
Chalmers University of Technology

Abstract

Porous media comprise a large range of natural and industrial materials and are typically complex on multiple length scales. At lower (micro-scopic) length scales, such media consist of a solid skeleton and fluid-filled pores in between. At higher (macro-scopic) length scales, transport of a migrating pore fluid can be observed in addition to the mechanical stress-strain response. The interaction between the pore fluid and the solid skeleton determines, in addition to the properties of the individual phases, the fully coupled response of the medium. Therefore, the investigation of macro-scale properties needs to take into account the processes between micro- and meso-scopic heterogeneities. This thesis investigates transport processes in porous media on multiple scales by applying computational homogenization and finite element simulation. Biot's equations of (linear) consolidation are introduced and combined with sharp and diffuse interface formulations that are established to investigate the effect of meso-scale heterogeneities, e.g. in form of fractures, on the overall material behavior. The scale transition of the heterogeneous porous meso-scale towards an homogeneous macro-scale problem is derived via Variationally Consistent Computational Homogenization.

Taking into account this modeling framework, the thesis investigates:
1) How the numerical modeling of heterogeneous porous media can be used to calibrate laboratory experiments.
2) How the fluid transport in fractured rock can be modeled by applying sharp and diffuse interface formulations.
3) How the effective diffusivity of porous media can be derived for the special case of three-phase concrete, where diffusion takes place preferably on interfaces in the structure. In this industrial porous material, fluid transport is not a relevant process but rather the diffusion of chloride ions in the fluid phase is of interest.

All in all, the thesis reveals limits and establishes possibilities by the numerical modeling of heterogeneities in porous media with the aim to provide a deeper understanding of the transport processes in porous media on multiple scales.

Keywords: Poroelasticity, Computational Homogenization, Fractured Rock, Three-Phase Concrete, Hydro-Mechanical Coupling

Science doesn't always go forwards. It's a bit like doing a Rubik's cube. You sometimes have to make more of a mess with a Rubik's cube before you can get it to go right.

Jocelyn Bell Burnell

Acknowledgements

The work in this thesis developed during my work at the Chalmers University of Technology in Gothenburg, Sweden, and at the Ruhr-Universität Bochum, Germany. Many people have contributed in some way or other and I hereby thank all of them for this.

First, I would like to express my gratitude to my main supervisor Prof. Dr.-Ing. Ralf Jänicke for sharing his expertise, for his advice and his wealth of ideas. Special thank for supporting me and for his flexibility notwithstanding the arising changes during my PhD program. Next, I would like to acknowledge Prof. Fredrik Larsson for his inspiring suggestions and for sharing his knowledge. Furthermore, I would like to thank Prof. Dr.-Ing. Holger Steeb, Prof. Dr. Jörg Renner, Prof. Kenneth Runesson and Dr. Beatriz Quintal for fruitful discussions and their interest in my work. Additionally, I would like to take the opportunity to thank the co-authors of the appended papers.

I would also like to thank my colleagues at the Division of Material and Computational Mechanics at Chalmers University of Technology as well as my former colleagues at the chair of continuum mechanics at Ruhr-Universität Bochum for the nice working environment, the hospitality and for sharing their experience.

Finally, I would like to thank my family and friends for their patience and support in this time. In particular Gabi and Martin for their untiring effort to share their enthusiasm concerning Geosciences. And special thank goes to Lars for being solid as a rock in turbulent times and all these years.

Thesis

This thesis consists of an extended summary and the following appended papers:

Paper A N. Pollmann, R. Janicke, J. Renner, and H. Steeb. "Numerical Investigation of the Effective Skempton Coefficient in Porous Rock Containing Fluid-Filled Fracture Networks". *Poromechanics VI*. With permission from ASCE. 2017, pp. 1420–1427

Paper B N. Pollmann, R. Jänicke, J. Renner, and H. Steeb. Experimental determination of the Skempton coefficient: Challenges and opportunities. *In review* (2019)

Paper C N. Pollmann, F. Larsson, K. Runesson, and R. Jänicke. Diffuse interface modeling and Variationally Consistent Homogenization of fluid transport in fractured porous media. *In review* (2019)

Paper D N. Pollmann, F. Larsson, K. Runesson, K. Lundgren, K. Zandi, and R. Jänicke. Modeling and computational homogenization of chloride diffusion in three-phase meso-scale concrete. *To be submitted for international publication* (2019)

The appended papers have been prepared in collaboration with the co-authors. The author of this thesis was the main responsible for the progress of the work. Namely, took part in planning of the papers and the development of the theory, carried out numerical implementation and simulations, and wrote major parts of the papers.

Contents

Part I
Extended Summary

1 Introduction

1.1 Motivation

The investigation and simulation of transport processes in porous media is important for various fields such as geomechanics, hydrology or even medical technologies. Porous media comprise a large range of natural or industrial materials with a broad spectrum of applications. The propagation of sound in porous, cancellous bone is important for medical technologies and among others analyzed in [24, 72]. The migration of immiscible liquids in porous media is important for environmental remediation [18]. Industrial porous media such as foams are e.g. used for leight-weight constructions [66], and the transport of chloride ions in reinforced concrete, a special case of porous media, is essential for building constructions and subject of ongoing research [40, 80, 84]. The fluid transport in fractured porous and fluid-saturated rock is e.g. of interest for oil- or gas-exploration as well as for geothermal energy and subject of several literature studies [62, 78]. During geothermal energy production, the rock is hydraulically stimulated, i.e. fractures are induced by the injection of water. These fractures enhance the conductivity of the rock which is a major part of efficient geothermal energy production. Moreover, the hydraulic stimulation of rock causes seismic attenuation in the reservoir which may result in large earthquakes as e.g. studied for a geothermal site in France in [7]. Additionally, it has been observed that seismic attenuation can be detected in hydrocarbon-saturated rock [6]. This seismic attenuation is found to be mainly caused by wave-induced fluid flow in fluid saturated, heterogeneous porous media [49, 60, 63]. This underlines the need for a suitable toolbox that is able to predict and assess seismic attenuation as well as to simulate and model the associated transport processes in porous media.
This thesis focuses on two main fields involving transport processes in porous media. First, the focus is set on fluid transport in fractured porous rock. Second, the chloride diffusion in porous concrete, which is important for a better understanding of the corrosion process of reinforced concrete, among others. The investigation of these processes requires to understand the underlying material on different scales.

1.2 Multi-scale modeling

An established method for the derivation of effective properties, i.e. overall macroscopic properties, e.g. for reservoir rock or for reinforced concrete constructions, is multi-scale modeling. In this approach, the material is analyzed on different scales as shown exemplary in Fig. 1.1. The multi-scale modeling involves typically two scales, the micro- and macro-scale. The macro-scale is the largest scale, such as the reservoir rock formation with a typical length scale L^{macro} of several hundred meters. This is the observable scale containing large heterogeneities, e.g. in form of faults or rock layers. On the other hand, the micro-scale has a characteristic length L^{micro} of several millimeters, where the micro-scale constituents such as solid grains and pore channels can be distinguished. In between these scales, a meso-scale with characteristic length L^{meso} has to be introduced, if heterogeneities of intermediate dimension are of interest.

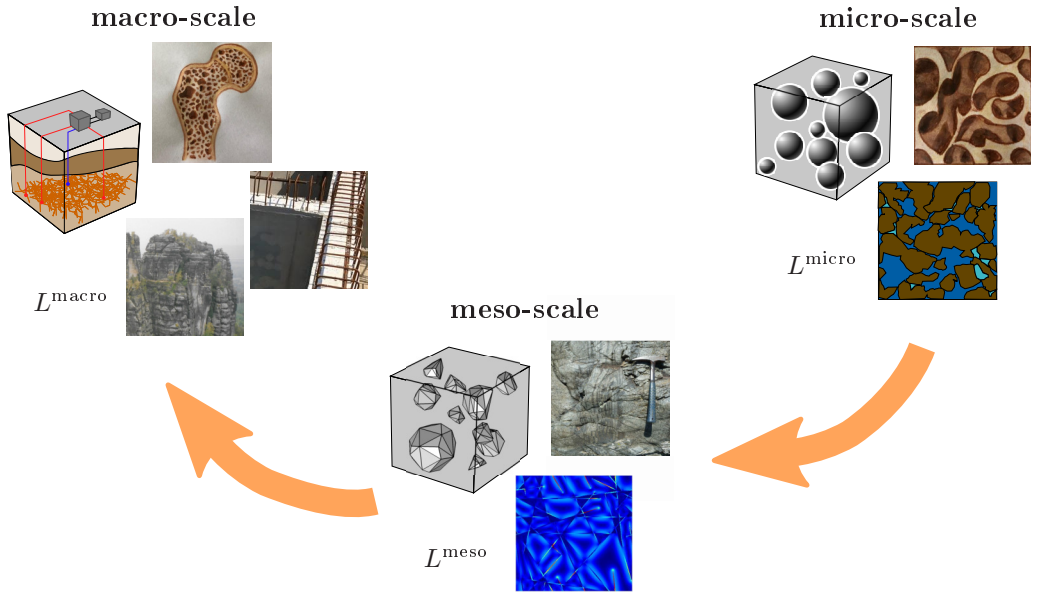

Figure 1.1: *Examples of material on different scales: Porous rock, porous concrete and porous bone on the micro-scale. Fractured rock and aggregate content in concrete on the meso-scale. Osteoporosis bone, geothermal reservoir, structure made from reinforced concrete and rock formation on the macro-scale.* $L^{micro} \ll L^{meso} \ll L^{macro}$.

The information on each of this scales is connected, i.e., the numerical modeling on the meso-scale requires information of the micro-scale, and overall macroscopic properties can only be derived taking into account the meso-scale problem. In this approach, the separation of scales is assumed, i.e. the characteristic length of the micro-scale is much smaller than the one of the meso-scale, whereas the characteristic length of the meso-scale is much smaller than the one of the macro-scale. Hence, $L^{\text{micro}} \ll L^{\text{meso}} \ll L^{\text{macro}}$. Multi-scale modeling can be applied in various areas of research and is an established method that has been investigated in a large and growing body of literature [30, 36, 69, 81]. In the studied cases, the micro- or meso-scale structure comprises heterogeneities such as fractures in rock or aggregate content in concrete. The pressure gradients between these meso-scale heterogeneities cause fluid flow and pressure diffusion. When studying wave propagation at the macro-scale, several studies in literature showed that the wave-induced fluid flow can be modeled using Biot's theory of poroelasticity [3, 14, 15, 63]. By assuming that the diffusion on the meso-scale is a local phenomenon, it is possible to describe the overall material on the macro-scale by means of a homogeneous, viscoelastic material. Thus, effective properties on this homogeneous macro-scale can be computed via Computational Homogenization [22, 29, 32, 38, 39, 67]. Here, the effective properties are obtained from homogenization over a meso-scale Representative Volume Element (RVE), typically chosen as a square or cubic domain of length L^{meso}. This RVE has to be large enough to be representative, i.e. to contain all necessary information and heterogeneities, but small

enough to allow for reasonably low computational effort. A possible, but not further discussed approach is the FE^2 approach studied in detail e.g. in [19, 52]. In this approach, the macro-scale problem and the RVE problem are solved in a nested fashion, i.e. the finite element method (FE) is used at both scales iteratively during the computation.

This thesis focuses on the modeling of the meso-scale structure in order to evaluate the macroscopic behavior without simultaneously solving the macroscopic problem. Two applications are studied in detail by using homogenization techniques. First, the scale transition between the meso-scale diffusion in fluid-saturated rock and the effective material behavior by means of the attenuation is performed. Second, the scale transition between diffusion of chloride ions in three-phase concrete and the macro-scale properties by means of the effective diffusivity is investigated.

1.3 Outline of the thesis

The main goal of this thesis is to elaborate on a suitable toolbox to simulate transport processes in porous media for the examples of rock and concrete. Therefore, the effect of fluid-filled fracture networks and of different aggregate shape, size and properties on the overall material properties of rock and concrete are investigated, respectively. One aspect of the study is the identification of possible advantages or disadvantages of numerical modeling compared to laboratory measurements of fluid-filled porous rock. An interpretation of a fracture model is investigated to study the applicability of the method to account for hydro-mechanical coupling processes.
The thesis starts with the characterization of the underlying material and the relevant processes in rock and concrete by introducing the Theory of Porous Media and Biot's theory of poroelasticity in Chapter 2. Chapter 3 investigates the numerical modeling of heterogeneities on the meso-scale by different approaches based on the introduced theoretical framework. Here, the fluid transport in fractured rock is analyzed by taking into account three different approaches. Additionally, the transport of chloride ions in concrete is investigated. In Chapter 4, Computational Homogenization is introduced for a prototype diffusion problem in a variationally consistent way. The thesis is completed with a summary of the appended papers A-D [54, 55, 56, 57] in Chapter 5 and finalized with the conclusions and outlook in Chapter 6.

2 Fluid transport in porous media

2.1 Preliminaries

The investigation of transport phenomena in porous media requires an adequate framework and knowledge of the underlying material. Porous media comprise a large variety of materials with various possible applications.
This thesis focuses on porous fractured rock and three-phase concrete. Concrete is an industrial porous material consisting of water, binder (cement), aggregates and chemical additives and its micro-structure can be analyzed e.g. by scanning electron microscope (SEM) [4, 13]. Porous rock, on the other hand, comprises a large range of rock types such as sedimentary rock (e.g. carbonate rock, clay, sandstone) or igneous rock (e.g. granite). The investigation of these media is of interest for many geoengineering applications as they often build oil- or gas reservoirs or serve as geothermal reservoir. Porous rock is characterized on the micro-scale as a multi-phase material consisting of solid grains and pore fluid in between, e.g. water (or a mixture of fluids). Specimens of the material can e.g. be analyzed experimentally by X-ray Computed Tomography [70], resulting in detailed information about the spatial distribution of the micro-scale constituents.

2.2 Mixture theory for biphasic media

The transport of fluid in porous rock includes, e.g., the transport of gas, chemicals or particles that are contained in the fluid-saturated rock. The presence of different constituents in the material results in a hydro-mechanical coupling with the need for a suitable modeling framework. These coupled processes can be described via multi-phase continua.
In this thesis, the focus lies on the investigation of biphasic media by means of the Theory of Porous Media, a phenomenologic, macroscopic theory. By means of a procedure similar to classical continuum mechanics, the constituents are averaged over a control volume Ω as shown in Fig. 2.1. On the micro-scale it is possible to distinguish between the solid skeleton, constituting the solid grains and the pore space including the pore fluid. By means of a homogenization these constituents are averaged resulting in a mixture. The two constituents of fluid-saturated rock are the solid and the pore fluid that are denoted by the subscript s and f, respectively. The superposition of the constituents φ^α, with $\alpha = \{\mathrm{s}, \mathrm{f}\}$ results in a description of the physical behavior of the mixture φ, given as

$$\varphi = \bigcup_\alpha \varphi^\alpha. \tag{2.1}$$

The mixture has to behave in accordance with the physical principles of its constituents. Therefore, an important information are the volume fractions of the constituents introduced as

$$n^\alpha = \mathrm{d}v^\alpha / \mathrm{d}v, \tag{2.2}$$

where the sum of the volume fractions $n_\mathrm{s} + n_\mathrm{f}$=1. The volume fractions can be used to derive an important property of the porous medium – the overall porosity, which can be distinguished between total and effective porosity. The first equals the volume fraction of the fluid ϕ_total=n_f, which is taken as the overall porosity ϕ in the conducted investigations. In contrast, the effective porosity ϕ_eff only includes the interconnected pore space [68]. The total control volume Ω is derived by the sum of the partial volumes as

$$V = |\Omega| = \int_\Omega \mathrm{d}v = \int_\Omega \mathrm{d}v^\mathrm{s} + \int_\Omega \mathrm{d}v^\mathrm{f}. \tag{2.3}$$

And similar the total mass is introduced as

$$M = \int_\Omega \mathrm{d}m = \int_\Omega \mathrm{d}m^\mathrm{s} + \int_\Omega \mathrm{d}m^\mathrm{f}. \tag{2.4}$$

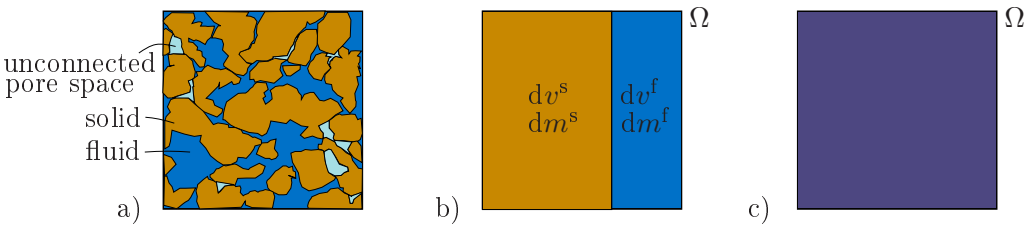

Figure 2.1: *Homogenization of porous rock on the micro-scale. a) Pore-scale, b) mixture theory, and c) continuum representation.*

Based on the partial mass of the constituents of the mixture it is possible to introduce the partial and true densities

$$\rho^\alpha = \frac{\mathrm{d}m^\alpha}{\mathrm{d}v} \qquad \rho^{\alpha\mathrm{R}} = \frac{\mathrm{d}m^\alpha}{\mathrm{d}v^\alpha}, \tag{2.5}$$

that are connected via their volume fractions according to

$$\rho^\alpha = n^\alpha \rho^{\alpha\mathrm{R}}. \tag{2.6}$$

On the basis of the introduced properties of the material, the aim is to find balance relations for the mixture. For more information concerning continuum and mixture theory, the interested reader is referred to [5, 10, 16, 23]. The derivation of the balance relations require the introduction of the related kinematics.

Kinematics: Similar to the single-phase continuum theory a motion function is introduced that connects the reference and the current configuration. At the time $t = t_0$ the material body Ω is in the reference configuration with separate reference points with position vectors $\mathbf{X}_\alpha$ of the fluid and solid constituent with $\alpha = \{\mathrm{f}, \mathrm{s}\}$, respectively.

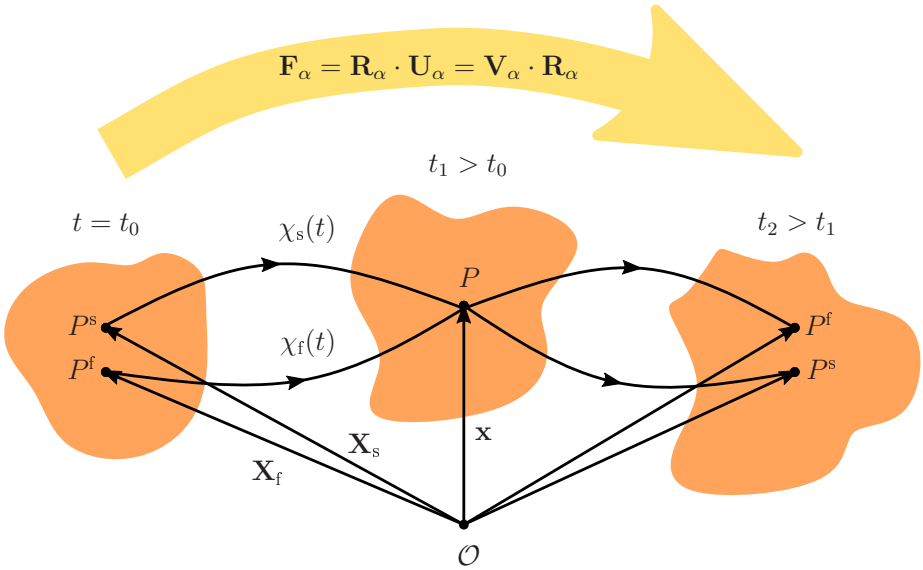

Figure 2.2: *State of motion of a biphasic continuum with solid and fluid constituents.*

By the effect of forces acting on Ω, the body moves into the current configuration at time t, as shown in Fig. 2.2. In doing so, the points follow their own motion functions $\boldsymbol{\chi}_\alpha$ towards the points at the current configuration. Here, each point with position vector $\mathbf{x}$ is simultaneously occupied by the particles of both constituents. This relation is described by

$$\mathbf{x} = \boldsymbol{\chi}_\alpha(\mathbf{X}_\alpha, t). \tag{2.7}$$

During the motion, the material points undergo displacement due to the coupled deformation (stretch $\mathbf{U}_\alpha$) and rotation ($\mathbf{R}_\alpha$) of the body resulting in the deformation gradient $\mathbf{F}_\alpha$ defined as

$$\mathbf{F}_\alpha := \frac{\partial \mathbf{x}}{\partial \mathbf{X}_\alpha} = \mathbf{R}_\alpha \cdot \mathbf{U}_\alpha. \tag{2.8}$$

To obtain a frame-invariant (objective) formulation, only the stretch tensor can effect the stored energy in the model. However, to calculate these tensors ($\mathbf{R}_\alpha$ and $\mathbf{U}_\alpha$) an eigenvalue problem has to be solved. To circumvent this issue, deformation and strain tensors are introduced. The right Cauchy-Green deformation tensor is defined with the polar decomposition as

$$\mathbf{C}_\alpha := \mathbf{F}_\alpha^T \cdot \mathbf{F}_\alpha = (\mathbf{R}_\alpha \cdot \mathbf{U}_\alpha)^T \cdot (\mathbf{R}_\alpha \cdot \mathbf{U}_\alpha) = \mathbf{U}_\alpha^T \cdot \mathbf{U}_\alpha. \tag{2.9}$$

And the Green-Lagrange strain tensor $\mathbf{E}_\alpha$ is derived by the difference of squares of the line elements as

$$\mathrm{d}s^2 - \mathrm{d}S_\alpha^2 = \mathrm{d}\mathbf{x} \cdot \mathrm{d}\mathbf{x} - \mathrm{d}\mathbf{X}_\alpha \cdot \mathrm{d}\mathbf{X}_\alpha = \mathrm{d}\mathbf{X}_\alpha \cdot \underbrace{(\mathbf{F}_\alpha^T \cdot \mathbf{F}_\alpha - \mathbf{I})}_{=:2\mathbf{E}_\alpha} \cdot \mathrm{d}\mathbf{X}_\alpha, \tag{2.10}$$

where $\mathrm{d}s$ and $\mathrm{d}S_\alpha$ are lengths in current and reference configuration, respectively.
The deformation gradient can be expressed by means of the displacement gradient and by making use of the displacement $\mathbf{u}_\alpha = \mathbf{x} - \mathbf{X}_\alpha$ as

$$\mathbf{F}_\alpha := \mathbf{x} \otimes \boldsymbol{\nabla}_{\mathbf{X}_\alpha} = \mathbf{I} + \mathbf{u}_\alpha \tag{2.11}$$

Throughout this thesis, only small deformations are assumed which allows for linearization of the strain tensor $\boldsymbol{\varepsilon}^\alpha[\mathbf{u}_\alpha] = \mathrm{lin}(\mathbf{E}(\mathbf{u}_0 = 0)) = (\mathbf{u}_\alpha \otimes \boldsymbol{\nabla})^{\mathrm{sym}}$. The velocity fields of the constituents are defined as

$$\mathbf{v}_\alpha := \frac{\partial \boldsymbol{\chi}(\mathbf{X}_\alpha, t)}{\partial t}. \tag{2.12}$$

$\mathbf{L}_\alpha$ transports line elements of the current configuration to the change of the elements by

$$\mathbf{L}_\alpha := \mathbf{v}_\alpha \otimes \boldsymbol{\nabla}_{\mathbf{x}} \tag{2.13}$$

and can be decomposed in a symmetric and unsymmetric part

$$\mathbf{D}_\alpha = \frac{1}{2}(\mathbf{L}_\alpha + \mathbf{L}_\alpha^T) \qquad \mathbf{W}_\alpha = \frac{1}{2}(\mathbf{L}_\alpha - \mathbf{L}_\alpha^T) \tag{2.14}$$

Balance relations: The guidelines for the formulation of the balance relations of mixtures are introduced by Truesdell [76] as metaphysical principles. Following these principles, the balance of mass, momentum, moment of momentum, energy and entropy are given subsequently.

The **balance of mass** reads

$$\frac{\mathrm{d}_\alpha}{\mathrm{d}t}[M^\alpha] = \hat{M}^\alpha = \frac{\mathrm{d}_\alpha}{\mathrm{d}t} \int_\Omega \rho^\alpha \mathrm{d}v = \int_\Omega \hat{\rho}^\alpha \mathrm{d}v, \tag{2.15}$$

with the mass production $\hat{M}^\alpha$. (2.15) can be transformed by making use of the transport of volume elements $\mathrm{d}v_\alpha = J_\alpha \mathrm{d}V$ using the Jacobian of each constituent and by localizing to

$$(\rho^\alpha)'_\alpha + \rho^\alpha(\boldsymbol{\nabla}_{\mathbf{x}} \cdot \mathbf{v}_\alpha) = \hat{\rho}^\alpha. \tag{2.16}$$

Here, the material time derivative is defined as

$$\bullet'_\alpha = \dot{\bullet} + (\bullet \otimes \boldsymbol{\nabla}_{\mathbf{x}}) \cdot \mathbf{v}_\alpha, \tag{2.17}$$

resulting in the localized, partial mass balance

$$\dot{\rho}^\alpha + \boldsymbol{\nabla}_{\mathbf{x}} \cdot (\rho^\alpha \mathbf{v}_\alpha) = \hat{\rho}^\alpha. \tag{2.18}$$

The global form of the mass balance, where the sum of the mass production vanishes, is given as a product of the mass balances of the pore fluid and the solid skeleton as

$$\dot{\rho} + \boldsymbol{\nabla}_{\mathbf{x}} \cdot (\rho \mathbf{v}) = 0. \tag{2.19}$$

The change of momentum of a constituent φ^α is balanced by the long- and short-range forces $\mathbf{F}^\alpha$ acting on it, and by the exchange of momentum $\hat{\mathbf{S}}^\alpha$. Thus, the **balance of momentum** is introduced as

$$[\mathbf{L}^\alpha]'_\alpha = \mathbf{F}^\alpha + \hat{\mathbf{S}}^\alpha, \tag{2.20}$$

where the momentum $\mathbf{L}^\alpha$, the forces $\mathbf{F}^\alpha$ and the interaction forces $\hat{\mathbf{S}}^\alpha$, respectively, are defined as

$$\mathbf{L}^\alpha = \int_\Omega \rho^\alpha \mathbf{v}_\alpha \mathrm{d}v, \qquad \mathbf{F}^\alpha = \int_\Omega \rho^\alpha \mathbf{b}^\alpha \mathrm{d}v + \int_\Gamma \mathbf{t}^\alpha \mathrm{d}a, \qquad \hat{\mathbf{S}}^\alpha = \int_\Omega \hat{\mathbf{s}}^\alpha \mathrm{d}v. \tag{2.21}$$

Inserting these relations in (2.20), applying the Cauchy-theorem $\mathbf{t}^\alpha = \mathbf{T}^\alpha \cdot \mathbf{n}$, where $\mathbf{T}^\alpha$ is the partial stress tensor and $\mathbf{n}$ is the outer normal vector. Localization of (2.20) leads to

$$\rho^\alpha \mathbf{a}_\alpha - \mathbf{T}^\alpha \cdot \boldsymbol{\nabla}_\mathbf{x} = \rho^\alpha \mathbf{b}^\alpha + \hat{\mathbf{p}}^\alpha. \tag{2.22}$$

Here, the direct momentum production term $\hat{\mathbf{p}}^\alpha = \hat{\mathbf{s}}^\alpha - \hat{\rho}^\alpha \mathbf{v}_\alpha$ is inserted as well as the acceleration field defined as

$$\mathbf{a}_\alpha := \frac{\partial^2 \boldsymbol{\chi}_\alpha(\mathbf{X}_\alpha, t)}{\partial t^2}. \tag{2.23}$$

Considering that the sum of the total momentum production of the fluid and solid constituent vanishes ($\hat{\mathbf{s}}^\mathrm{s} + \hat{\mathbf{s}}^\mathrm{f} = 0$), the momentum balance of the biphasic mixture is defined as

$$\rho \mathbf{a} - \mathbf{T} \cdot \boldsymbol{\nabla}_\mathbf{x} = \rho \mathbf{b}, \tag{2.24}$$

where mass production of the biphasic mixture is assumed to vanish according to

$$\sum_\alpha \hat{\rho}^\alpha \mathbf{v}_\alpha = 0. \tag{2.25}$$

Hereby, the stress of the mixture is computed as

$$\mathbf{T} = \sum_\alpha \mathbf{T}^\alpha. \tag{2.26}$$

the density ρ, the acceleration $\mathbf{a}$ and the body forces $\rho\mathbf{b}$ of the mixture are computed accordingly.
The energy of a constituent φ^α of a material body Ω is changed by the mechanical and thermal power and, in addition, the exchange of energy between the constituents. The **balance of energy** is given in the global form as

$$[E^\alpha + K^\alpha]'_\alpha = P^\alpha_\mathrm{ext} + Q^\alpha + \hat{E}^\alpha. \tag{2.27}$$

It contains the internal E^α and kinetic energy K^α, the stress power P^α_ext, the thermal power Q^α depending on the heat flux $\mathbf{q}^\alpha$, and the partial energy production $\hat{E}^\alpha$ defined

as

$$E^\alpha = \int\limits_\Omega \rho^\alpha \varepsilon^\alpha \mathrm{d}v, \tag{2.28a}$$

$$K^\alpha = \int\limits_\Omega \frac{1}{2}\rho^\alpha \mathbf{v}_\alpha \cdot \mathbf{v}_\alpha \mathrm{d}v, \tag{2.28b}$$

$$P^\alpha_{\mathrm{ext}} = \int\limits_\Gamma \mathbf{t}^\alpha \cdot \mathbf{v}_\alpha \mathrm{d}a + \int\limits_\Omega \rho \mathbf{b}^\alpha \cdot \mathbf{v}_\alpha \mathrm{d}v, \tag{2.28c}$$

$$Q^\alpha = \int\limits_\Gamma \mathbf{q}^\alpha \mathrm{d}a + \int\limits_\Omega \rho^\alpha r^\alpha \mathrm{d}v, \tag{2.28d}$$

$$\hat{E}^\alpha = \int\limits_\Omega \hat{\varepsilon}^\alpha \mathrm{d}v. \tag{2.28e}$$

Using standard argumentation with Reynold's transport theorem, Cauchy and Gauss integral rule, the local form of the balance of energy is derived. This balance equation can be split to obtain the local form of balance of kinetic energy

$$\frac{1}{2}\left[\mathbf{v}_\alpha \cdot \mathbf{v}_\alpha\right]'_\alpha = (\mathbf{T}^\alpha \cdot \mathbf{v}_\alpha) \cdot \boldsymbol{\nabla}_{\mathbf{x}} - \mathbf{T}^\alpha : \mathbf{D}_\alpha + \rho^\alpha \mathbf{v}_\alpha \cdot \mathbf{b}^\alpha + \mathbf{v}_\alpha \cdot \hat{\mathbf{p}}^\alpha \tag{2.29}$$

and the local form of the balance of internal energy

$$\rho^\alpha (\varepsilon^\alpha)'_\alpha = \mathbf{T}^\alpha : \mathbf{D}_\alpha - \mathbf{q}^\alpha \cdot \boldsymbol{\nabla}_{\mathbf{x}} + \rho^\alpha r^\alpha + \hat{\varepsilon}^\alpha - \mathbf{v}_\alpha \cdot \hat{\mathbf{p}}^\alpha, \tag{2.30}$$

with the algebraic constraint that the sum of energy production $\hat{e}^\alpha$ vanishes. Thus the energy balances of the mixture are obtained as

$$\frac{1}{2}\left[\mathbf{v} \cdot \mathbf{v}\right]' = (\mathbf{T} \cdot \mathbf{v}) \cdot \boldsymbol{\nabla}_{\mathbf{x}} - \mathbf{T} : \mathbf{D} + \rho \mathbf{v} \cdot \mathbf{b}, \tag{2.31a}$$

$$\rho \varepsilon' = \mathbf{T} : \mathbf{D} - \mathbf{q} \cdot \boldsymbol{\nabla}_{\mathbf{x}} + \rho r. \tag{2.31b}$$

Thermodynamic processes are in general irreversible. Thus, the thermal energy cannot be fully transformed to mechanical energy. This can be described by the **balance of entropy**

$$\left[S^\alpha\right]'_\alpha = H^\alpha + \hat{R}^\alpha, \tag{2.32}$$

with

$$S^\alpha = \int\limits_\Omega \rho^\alpha \eta^\alpha \mathrm{d}v \tag{2.33a}$$

$$H^\alpha = -\int\limits_\Gamma \boldsymbol{\phi}^\alpha_\eta \cdot \mathbf{n} \mathrm{d}a + \int\limits_\Omega \rho^\alpha s^\alpha_\eta \mathrm{d}v \tag{2.33b}$$

$$\hat{R}^\alpha = \int\limits_\Omega \hat{\eta}^\alpha \mathrm{d}v. \tag{2.33c}$$

In local form, related to the quantities of the current configuration, the entropy balance is defined as

$$\rho^\alpha (\eta^\alpha)'_\alpha + \boldsymbol{\nabla}_{\mathbf{x}} \cdot \boldsymbol{\phi}^\alpha_\eta - \rho^\alpha s^\alpha_\eta = \hat{\xi}^\alpha, \tag{2.34}$$

where the total entropy production $\hat{\eta}^\alpha$ can be related to the direct entropy product $\hat{\xi}^\alpha$ as

$$\hat{\eta}^\alpha = \hat{\xi}^\alpha + \eta^\alpha \hat{\rho}^\alpha. \tag{2.35}$$

The entropy principle is formulated for the mixture as

$$\sum_\alpha \hat{\eta}^\alpha \geq 0. \tag{2.36}$$

All balance relations result in a system of equations including also the balance of moment of momentum. As this thesis focuses on the modeling of biphasic poroelastic media under several restrictions, the discussion of all balance relations with associated relations is not further discussed and can be found in literature.

2.3 Biot's equations of linear consolidation

In case of a biphasic medium, an established approach to study the hydro-mechanical interactions, is the theory of poroelasticity or consolidation [2, 3, 9, 12, 74, 77, 79], which is based on the concept of the coupling between the deformation of the solid and the flow of pore fluid, building the two constituents of the biphasic mixture. If the solid skeleton, consisting of solid grains, undergoes a deformation, the pore space in between undergoes a volume change or vice versa, which causes flow of the pore fluid due to pressure gradients. This results in fluid flow on the micro-scale e.g. in micro-cracks known as squirt-flow [62]. Here, no mass exchange occurs and isothermal conditions are assumed. Additionally, the Cauchy stress tensors $\mathbf{T}, \mathbf{T}^{\alpha}$ can be replaced by $\boldsymbol{\sigma}, \boldsymbol{\sigma}^{\alpha}$. Moreover, body- as well as inertia forces can be neglected resulting in a quasi-static description of the partial momentum balance of (2.22) as

$$-\boldsymbol{\sigma}^{\mathrm{s,f}} \cdot \boldsymbol{\nabla} - \hat{\mathbf{p}}^{\mathrm{s,f}} = \mathbf{0}. \tag{2.37}$$

Here, the direct momentum production term vanishes by excluding phase transition between the two constituents and neglecting mass production, i.e.

$$\hat{\mathbf{p}}^{\mathrm{s}} + \hat{\mathbf{p}}^{\mathrm{f}} = \hat{\mathbf{s}}^{\mathrm{s}} + \hat{\mathbf{s}}^{\mathrm{f}} - \underbrace{(\hat{\rho}^{\mathrm{s}}\mathbf{v}_{\mathrm{s}} + \hat{\rho}^{\mathrm{f}}\mathbf{v}_{\mathrm{f}})}_{\text{no mass production}} = \mathbf{0}. \tag{2.38}$$

The formulation of the total momentum balance requires constitutive relations for the two constituents. The solid phase (skeleton) is modeled as linear elastic and isotropic material by Hooke's law, resulting in the constitutive relation

$$\boldsymbol{\sigma}^{\mathrm{s}}_{\mathrm{E}} := \mathbb{E} \colon \boldsymbol{\varepsilon}[\mathbf{u}] = 2\,G\,\boldsymbol{\varepsilon} + \left(3K - \frac{2}{3}G\right)\,\mathrm{tr}\,(\boldsymbol{\varepsilon})\mathbf{I}, \tag{2.39}$$

where the linear solid strain $\boldsymbol{\varepsilon}[\mathbf{u}] := (\mathbf{u} \otimes \boldsymbol{\nabla})^{\mathrm{sym}}$ is computed from the displacement of the solid phase $\mathbf{u}$. For the restriction to the linear case, the gradient operator is defined as $\boldsymbol{\nabla}\bullet = \partial\,\bullet\,/\partial\mathbf{x}$ assuming that the gradient operator with respect to the current position equals the gradient operator with respect to the reference position. K and G are the bulk and shear modulus of the dry skeleton, respectively. The effective stress $\boldsymbol{\sigma}^{s}_{\mathrm{E}}$ of the solid skeleton is connected to the pore pressure p of the fluid phase in form of the total stress

$$\boldsymbol{\sigma} = \boldsymbol{\sigma}^{\mathrm{s}} + \boldsymbol{\sigma}^{\mathrm{f}} = \boldsymbol{\sigma}^{\mathrm{s}}_{\mathrm{E}} - \alpha\,p\,\mathbf{I}, \tag{2.40}$$

where

$$\boldsymbol{\sigma}^{\mathrm{f}} = -\phi\,p\,\mathbf{I}, \tag{2.41a}$$
$$\boldsymbol{\sigma}^{\mathrm{s}} = \boldsymbol{\sigma}^{\mathrm{s}}_{\mathrm{E}} - (\alpha - \phi)p\,\mathbf{I}, \tag{2.41b}$$

Here $\alpha = 1 - K/K^{s}$ is the Biot-Willis coefficient with the bulk modulus of the solid grains K^{s}. The two field variables are the displacement $\mathbf{u}$ of the solid skeleton and the pressure p of the pore fluid. To be able to solve the problem for these two variables an additional equation is required, resulting in the $\mathbf{u}$-p-formulation [61] for the numerical derivation.

In the theory of consolidation the mass of the solid and the fluid constituent has to be conserved. Therefore the partial mass balance of (2.18) is recalled

$$(\rho^{\mathrm{s,f}})'_{\mathrm{s,f}} + \rho^{\mathrm{s,f}} \boldsymbol{\nabla} \cdot \mathbf{v}_{\mathrm{s,f}} = 0. \tag{2.42}$$

Here, the material time derivative of (2.17) is applied and the velocity of the fluid phase can be expressed by the relative velocity related to the solid phase. i.e. $\mathbf{v}_{\mathrm{f}} = \mathbf{w}_{\mathrm{f}} + \mathbf{v}_{\mathrm{s}}$ resulting in the partial mass balances for the fluid and solid, respectively

$$(\rho^{\mathrm{f}})'_{\mathrm{f}} + \rho^{\mathrm{f}} \boldsymbol{\nabla} \cdot \mathbf{w}_{\mathrm{f}} + \rho^{\mathrm{f}} \boldsymbol{\nabla} \cdot \mathbf{v}_{\mathrm{s}} = 0, \tag{2.43a}$$

$$(\rho^{\mathrm{s}})'_{\mathrm{s}} + \rho^{\mathrm{s}} \boldsymbol{\nabla} \cdot \mathbf{v}_{\mathrm{s}} = 0. \tag{2.43b}$$

The material time derivative of the partial densities can be obtained by using the assumption of linear consolidation as $(\rho^{\mathrm{s,f}})'_{\mathrm{s,f}} = \dot{\rho}^{\mathrm{s,f}}$. Additionally, (2.6) is taken into account, i.e. $\rho^{\mathrm{s,f}} = n^{\mathrm{s,f}} \rho^{\mathrm{s,fR}}$, for a biphasic mixture, where the volume fractions can be expressed by the use of the porosity as $n^{\mathrm{f}} = \phi$, $n^{\mathrm{s}} = 1 - \phi$. The constitutive relations for the densities are defined in accordance with [77] as

$$\dot{\rho}^{\mathrm{fR}} = \frac{\rho^{\mathrm{fR}}}{K^{\mathrm{f}}} \dot{p}, \tag{2.44a}$$

$$\dot{\rho}^{\mathrm{sR}} = \frac{1}{K^{\mathrm{s}}} \frac{\rho^{\mathrm{sR}}}{1-\phi} (-\dot{\sigma} - \phi \dot{p}). \tag{2.44b}$$

Here, K^{f} is the bulk modulus of the fluid and $\dot{\sigma}$ is the rate of the mean stress $\sigma = 1/3 \mathrm{tr}\, \boldsymbol{\sigma}$ that can be related to the volume strain. These correlations are inserted in (2.43) to obtain

$$\phi \frac{\dot{p}}{K^{\mathrm{f}}} + \dot{\phi} + \phi \, \boldsymbol{\nabla} \cdot \mathbf{w}_{\mathrm{f}} + \phi \, \boldsymbol{\nabla} \cdot \mathbf{v}_{\mathrm{s}} = 0 \qquad \text{for the fluid,} \tag{2.45a}$$

$$-\dot{\phi} + \frac{1}{K^{\mathrm{s}}} (-\dot{\sigma} - \phi \dot{p}) + (1-\phi) \boldsymbol{\nabla} \cdot \mathbf{v}_{\mathrm{s}} = 0 \qquad \text{for the solid.} \tag{2.45b}$$

Adding these equations under the consideration that $\dot{\sigma} = K \boldsymbol{\nabla} \cdot \dot{\mathbf{u}} - \alpha \dot{p}$, finally results in

$$\underbrace{\left(\frac{\phi}{K^{\mathrm{f}}} + \frac{\alpha - \phi}{K^{\mathrm{s}}} \right)}_{=:\beta} \dot{p} + \underbrace{\phi \boldsymbol{\nabla} \cdot \mathbf{w}_{\mathrm{f}}}_{=:\boldsymbol{\nabla} \cdot \mathbf{w}} + \boldsymbol{\nabla} \cdot \mathbf{v}_{\mathrm{s}} \underbrace{\left(-\frac{K}{K^{\mathrm{s}}} + 1 \right)}_{=:\alpha} = 0. \tag{2.46}$$

The flow of the pore fluid is given by the linear assumption of Darcy's law as

$$\mathbf{w} := -\mathbf{K} \cdot \boldsymbol{\zeta}[p], \qquad \boldsymbol{\zeta}[p] = \boldsymbol{\nabla} p. \tag{2.47}$$

Here, the second order permeability tensor $\mathbf{K}$ is derived in the case of isotropy as $\mathbf{K} = k/\eta \, \mathbf{I}$, where k and η are the permeability of the material and the effective dynamic viscosity of the pore fluid, respectively.
Taking into account balance of mass of the fluid and balance of momentum of the mixture given by (2.18) and (2.24), Biot's quasi-static equations including boundary conditions

can be formulated. Here the aim is to derive the displacement field $\mathbf{u}(\mathbf{x},t) : \Omega \times \mathbb{R}^+ \to \mathbb{R}^3$ and the pore pressure field $p(\mathbf{x},t) : \Omega \times \mathbb{R}^+ \to \mathbb{R}$ for the system

$$-\boldsymbol{\sigma}(\boldsymbol{\varepsilon}[\mathbf{u}], p) \cdot \boldsymbol{\nabla} = \mathbf{0} \qquad \text{in } \Omega \times (0,T], \tag{2.48a}$$

$$\mathbf{u} = \mathbf{u}^{\mathrm{p}} \qquad \text{on } \Gamma_{\mathrm{D}}^{(u)} \times (0,T], \tag{2.48b}$$

$$\mathbf{t} := \boldsymbol{\sigma} \cdot \mathbf{n} = \mathbf{t}^{\mathrm{p}} \qquad \text{on } \Gamma_{\mathrm{N}}^{(u)} \times (0,T], \tag{2.48c}$$

$$\dot{\Phi}(\boldsymbol{\varepsilon}[\mathbf{u}], p) + \mathbf{w}(\boldsymbol{\zeta}[p]) \cdot \boldsymbol{\nabla} = 0 \qquad \text{in } \Omega \times (0,T], \tag{2.48d}$$

$$p = p^{\mathrm{p}} \qquad \text{on } \Gamma_{\mathrm{D}}^{(p)} \times (0,T], \tag{2.48e}$$

$$w := \mathbf{w} \cdot \mathbf{n} = w^{\mathrm{p}} \qquad \text{on } \Gamma_{\mathrm{N}}^{(p)} \times (0,T]. \tag{2.48f}$$

where $\dot{\Phi}(\boldsymbol{\varepsilon}[\mathbf{u}], p)$ is the time-derivative of the storage function given as

$$\Phi(\boldsymbol{\varepsilon}[\mathbf{u}], p) = \phi + \alpha \mathbf{I} : \boldsymbol{\varepsilon}[\mathbf{u}] + \beta p. \tag{2.49}$$

Here, $\beta = \phi/K^f + (\alpha - \phi)/K^s$ is the storativity, where K^f is the bulk modulus of the pore fluid.
The set of partial differential equations(2.48) contains the coupling of the deformation of the solid phase and the pressure diffusion of the pore fluid within, resulting in an $\mathbf{u}$-p-formulation. This fundamental equations provide a useful toolbox for the modeling of heterogeneous porous rock. Thus, Biot's equations are numerically solved with the finite element program Comsol Multiphysics. They can be combined with suitable model assumptions for fluid transport in meso-scale fractures or uncoupled in form of a 1-dimensional diffusion equation, as discussed in Chapter 3.

3 Porous media with meso-scale heterogeneities

This chapter investigates the effect of heterogeneities in porous media on the overall behavior. The focus is set on the numerical modeling of the hydro-mechanical interaction between fractures and the surrounding matrix. Afterwards, the ion diffusion in meso-scale concrete is discussed as a special case of a diffusion process in porous media.

3.1 Heterogeneous poroelastic materials

Wave-induced fluid flow is mainly caused by pressure gradients between heterogeneities. This process is modeled using Biot's theory as explained in detail in Chapter 2. The interaction of the solid skeleton and the pore fluid of fluid-saturated porous rock results in an apparently viscoelastic material behavior. That is, the behavior takes place between the two extremes of flow of ideal viscous fluid (pore water) and the deformation of ideal elastic solid (skeleton). In contrast to a pure elastic solid, the material response on a cyclic loading is frequency dependent in this case, resulting in frequency-dependent attenuation. In the low-frequency range, the observed attenuation is called seismic attenuation, which can e.g. be observed during geological exploration.
Typical examples of meso-scale heterogeneities in poroelastic material resulting in seismic attenuation are e.g. described by patchy saturation or double porosity models. Patchy saturation describes regions saturated with different fluids. The fluid flow between these regions is subject of a considerable amount of literature, [33, 43] to name but a few.
A 1-dimensional layered model was introduced by White et al. and studied in numerous works [14, 15, 82, 83]. The model has also been extended towards a 3-dimensional spherical patchy saturation model of a sphere embedded in a cubic matrix. The double porosity model, studied e.g. by [58, 59, 60] assumes that the material consists of regions with different poroelastic material properties, but saturated by one fluid. In paper A and B this assumption is chosen in order to transfer and quantify results from numerical investigation of different setups towards laboratory measurements. The models can be substituted by viscoelastic material models, i.e. by a combination of elastic and viscous element, resulting in storage and loss module. Theses modules can be evaluated in form of the phase velocity and the attenuation (tangent of phase angle) quantified by the inverse, frequency dependent quality factor $1/Q$.
Although, the models discussed above have to be highly complex to properly reflect the attenuation behavior of the medium. This can be shown by means of an example, such as the modified Cryer model, which represents a simple 1-dimensional consolidation problem. Here, a poroelastic and fully fluid-saturated sphere consisting of two domains with different material parameter is studied under constant hydrostatic stress and drained boundary conditions as shown in Fig. 3.1 a) [11, 55]. It can be shown that the attenuation of this example in form of the inverse quality factor computes in the low-frequency limit as the frequency and in the high-frequency limit by $1/\sqrt{(}f)$ as shown in Fig. 3.1 b). A viscoelastic material model such as the three-parameter Maxwell-Zener model [23], consisting of a

more advanced combination of damper and springs, shows a comparable attenuation behavior. Nevertheless, the high-frequency domain for this model is proportional to $1/f$, contrary to the actual attenuation behavior of the Cryer model. This shows, that even for this simple example complex viscoelastic models have to be considered to capture the process properly. One possibility is numerical simulation of meso-scale poroelasticity.

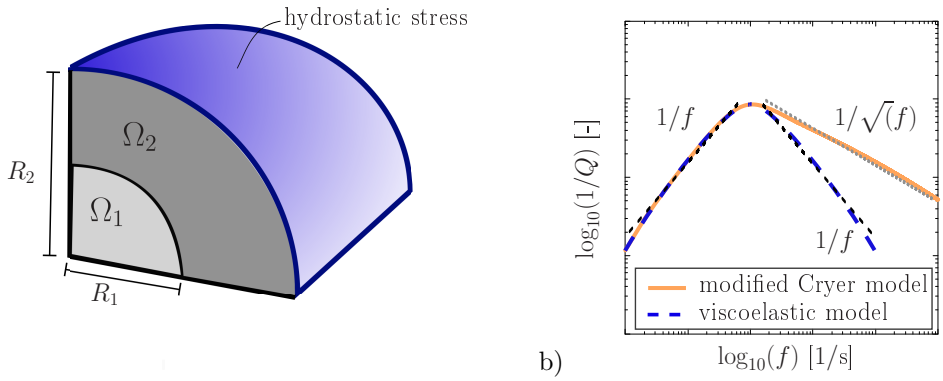

Figure 3.1: *a) Modified Cryer model: Layered structure of poroelastic domains* Ω_1 *and* Ω_2 *with different material parameters. b) Attenuation 1/Q versus frequency.*

For instance the seismic attenuation can be studied by means of the $\mathbf{u}$-p-formulation in form of transient stress relaxation or creeping test, resulting in the time-dependent stress-strain response. This presents an established method to calculate attenuation due to wave-induced fluid flow [42]. The frequency dependent effective stress and strain rates are computed applying a Fast Fourier Transform (FFT) as explained in detail in [63] and can be used to compute the inverse quality factor.
Another interesting factor which can be investigated by the introduced methods is the Skempton coefficient B. It presents an important factor for linear poroelasticity and can be derived analytically [14, 60]. It quantifies the ratio of changes in fluid pressure by change of mean stress σ^{M} for undrained conditions ($\boldsymbol{\nabla} \cdot \mathbf{u} = 0$) and is defined as

$$B = -\left.\frac{\partial p}{\partial \sigma^M}\right|_{\boldsymbol{\nabla}\cdot\mathbf{u}=0} \qquad \sigma^M = \frac{1}{3}\mathrm{tr}\,\boldsymbol{\sigma}. \tag{3.1}$$

The simple heterogeneity problems are developed in the following section to account for more complex meso-scale heterogeneities in porous media, such as fractures.

3.2 Poroelastic materials with fractures

Fluid transport in fractured porous rock is an important topic for many geoengineering applications. The characterization of natural and (hydraulically) induced fractures as well as the propagation of these is an important issue e.g. in case of hydraulic stimulation for geothermal energy production or gas- and oil-exploration. Therefore, it is essential to

understand the hydro-mechanically processes in fractured rock.
This thesis investigates attenuation processes in stationary (i.e. not evolving) fracture networks to analyze the hydro-mechanically driven fluid flow in fractured porous rock. This allows to draw conclusions e.g. on the hydraulic conductivity of the fracture networks. This is essential for the interpretation of data of seismic exploration, one of the key factors for the decision concerning suitable reservoirs for geothermal energy production.
The numerical investigation of fluid flow in fractured poroelastic rock requires numerical models for the fractures. Fractures in porous rock often represent thin regions (conduits) filled with fluid that cause higher permeability. Their (fracture) aperture is much smaller than their length. In this thesis, the fractures are assumed to be mechanically and hydraulically open. They constitute fracture networks that allow for an increased fluid flow in contrast to the fluid flow in the background material. Fracture networks can be highly heterogeneous with varying fracture apertures and varying fracture orientations. They may also occur on different length scales [28].
Different approaches for the numerical modeling of these fracture networks have been discussed in literature [46, 48, 63, 65, 78]. In the following, the focus lies on three of them: First, the fracture characterization as poroelastic fractures is investigated as a special case of patchy saturation. Second, a sharp interface model is introduced and third, the fractures are modeled in a diffuse fashion. An additional approach which is discussed in literature, is the implementation of Navier-Stokes and Lamé-Navier equations, where the rock is treated as linear elastic material containing fractures filled with a compressible and viscous fluid [1].

Patchy saturation: Biot's theory of poroelasticity is applied to define a rock containing heterogeneities with extreme geometrical and physical parameters, considered as fractures. Both, the fractures and the rock, are modeled as poroelastic domains saturated by the same fluid. The fractures are modeled as homogeneous and isotropic poroelastic patches with high porosity, high permeability and low stiffness. The main advantage is that no additional equation for the flow of fluid in the fractures is necessary. Additionally, the transition conditions between the fractures and the surrounding matrix are simply continuity conditions for the field variables (solid displacement and pore pressure). The fractures can be stochastically generated and arranged in a periodic manner which is advantageous for Computational Homogenization as discussed in Chapter 4.
The 2-dimensional control volumes contain fractures that are modeled as ellipses with low fracture aperture in contrary to their length. A 2-dimensional setup is chosen in order to reduce numerical costs contrary to a 3-dimensional setup. The elliptic description of the fractures is chosen to avoid singularities caused by vertices at the fracture tips. In Fig. 3.2 a) different examples of fracture networks are presented. The variation of the fracture length $2a$ as well as of the fracture aperture τ allows to study different aspects of the fracture network. Biot's equations (2.48) are numerically solved in the finite element program Comsol Multiphysics. For this purpose, the equation system has to be transformed into its weak format.

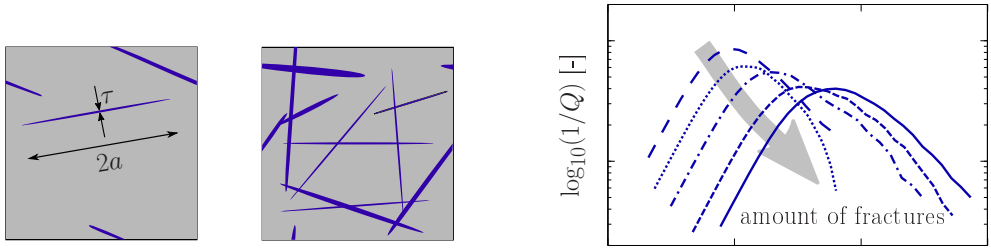

a) b)

Figure 3.2: *a) Examples of control volumes containing periodic fracture networks. b) Inverse quality factor versus frequency for varying amount of fractures. More fractures lead to lower magnitude and higher frequency*

The weak form of the system with the aim to find $\mathbf{u}(\mathbf{x},t), p(\mathbf{x},t)$ in the appropriately defined spaces $\mathbb{U} \times \mathbb{P}$ reads

$$\int_\Omega \left(\boldsymbol{\varepsilon}[\mathbf{u}] \colon \mathbb{E} \colon \boldsymbol{\varepsilon}[\delta\mathbf{u}] - \alpha p \mathbf{I} \colon \boldsymbol{\varepsilon}[\delta\mathbf{u}]\right) \mathrm{d}\Omega = \int_{\Gamma_\mathrm{N}^{(u)}} \mathbf{t}^\mathrm{p} \cdot \delta\mathbf{u} \, \mathrm{d}\Gamma \quad \forall \delta\mathbf{u} \in \mathbb{U}^0, \tag{3.2a}$$

$$\int_\Omega \left(\alpha \mathbf{I} \colon \boldsymbol{\varepsilon}[\dot{\mathbf{u}}]\delta p + \beta \dot{p}\delta p + \boldsymbol{\nabla} p \cdot \mathbf{K} \cdot \boldsymbol{\nabla}\delta p\right) \mathrm{d}\Omega = -\int_{\Gamma_\mathrm{N}^{(p)}} w^\mathrm{p} \delta p \, \mathrm{d}\Gamma \quad \forall \delta p \in \mathbb{P}^0, \tag{3.2b}$$

together with the initial condition

$$\Phi = \Phi^\mathrm{p} \qquad \text{in } \Omega \text{ at } t = 0. \tag{3.3}$$

$\mathbb{U}^0, \mathbb{P}^0$ are appropriately defined test spaces.
Taking these model equations into account, the effect of the meso-scale heterogeneities on macro-scale properties is investigated, as shown exemplarily in Fig. 3.2 b) by means of the inverse quality factor derived for a control volume with varying amount of fractures. It shows the typical behavior of low- and high- frequency range and the attenuation peak. The peak represents the point of highest attenuation, i.e. the transition zone. At the thereto related critical frequency, the relaxation process occurs. As can be seen in Fig. 3.2 b), the attenuation peak is shifted towards higher frequencies, while the attenuation peak tends to decrease, for increasing amount of fractures. Thus, it can be shown that the meso-scale heterogeneities in form of fractures affect the macro-scale attenuation. Due to the fact that this seismic attenuation is mostly caused by wave-induced this fluid flow on the meso-scale domain, these fluid flow processes are of interest. In this setup, the different mechanisms of fluid flow on the meso-scale are: 1) fracture flow, i.e. flow within the fractures, 2) matrix diffusion, i.e. processes of pressure redistribution in the poroelastic surrounding rock and 3) leak-off, describing the effect of mass exchange between fractures and matrix. All flow processes are captured by applying the model formulation of patchy saturation on meso-scale fracture networks in form of thin patches. It can be shown that the size of these patches, varied by aspect ratio and length, strongly effects the macro-scale attenuation. Therefore, this investigation points towards interpretation of

data from reservoir monitoring.
The numerical modeling of fractured rock with the application of the patchy saturation method has several advantages. The numerical modeling via the **u**-p-formulation includes consistent boundary conditions for the two field variables, resulting in the ability to model complex fracture networks with unstructured meshes for the FE. Another advantage, due to the implementation with FE, is that the computation of variable time-steps is possible. The approach provides a useful tool for an efficient modeling of hydro-mechanical processes on the meso-scale, e.g. with the aim to quantify and to transfer results to experimental measurements. Though, the aspect ratio of the ellipses that represent the fractures has to be moderate with $2a/\tau \leq 1000$ caused by the numerical limits of the meshing and the number of degrees of freedom. Additionally, the approach does not consider the hydro-mechanical coupling at lower dimensions such as caused by dead-end pores. These pores on the micro-scale do not deform during the fluid flow as described in detail in [37].

Sharp interface formulation: To account for very thin fractures, i.e. geological breaks [28] that are characterized by the fact that their length is significantly larger than their local aperture, a sharp interface model is presented subsequently. This section introduces the model assumptions and gives a brief summary. More details can be found in paper C and in the literature [31, 78]. In this approach, the fractures are modeled as sharp interfaces embedded in a fully fluid-saturated poroelastic rock matrix. The fractures are modeled as 1-dimensional (2-dimensional) interfaces in a 2-dimensional (3-dimensional) control volume as shown in Fig. 3.3 a).

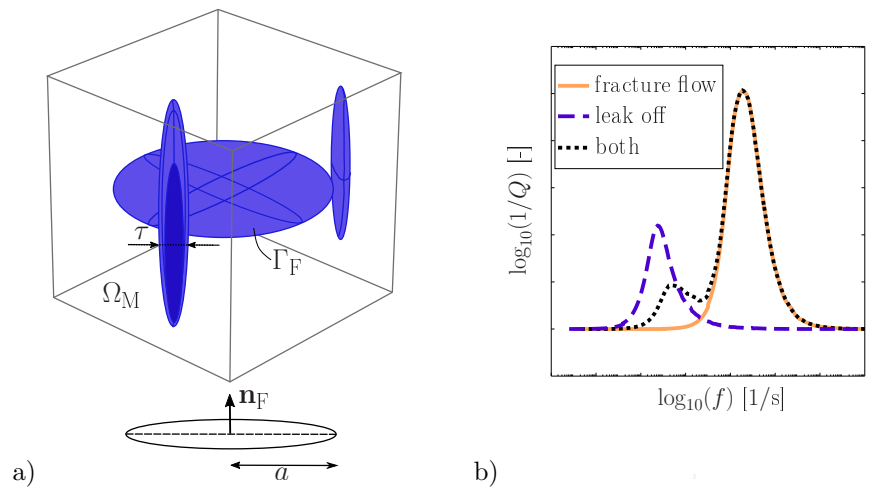

Figure 3.3: *Sharp interface model. a) 2-dimensional fractures with fracture aperture $\tau(\boldsymbol{x}, t)$ in a 3-dimensional domain Ω_M. b) Fluid-flow mechanisms in between the fractures and from fracture to surrounding matrix.*

Thus, the fractures are lower-dimensional interfaces with the material parameter τ defined as the fracture aperture. The matrix is modeled consisting of solid grains and the pore fluid within, by applying the $\mathbf{u}$-p-formulation for the domain Ω_{M} and Γ_{F}. Here, the pressure in the matrix is denoted p_{M}. The flow of pore fluid in the fractures is obtained by combining the balance of mass and balance of momentum in form of a Poiseuille-type flow rule [1] in the fracture domain Γ_{F}. Due to the dimensional reduction of the fractures, the fracture domain reduces to an interface (ellipse) with fracture opening τ. The fracture network consists of n_{F} fractures, where $\Gamma_{\mathrm{F}} = \bigcup_{\mathrm{i}=1}^{n_{\mathrm{F}}} \Gamma_{\mathrm{F_i}}$. To couple the Poiseuille-type flow in the dimensional reduced fractures with the poroelastic background, Biot's equations (2.48) are enhanced by a continuity equation for Γ_{F}.
The aim is to find the solid displacement field $\mathbf{u}(\mathbf{x},t) : \Omega_{\mathrm{M}} \times \mathbb{R}^+ \to \mathbb{R}^3$, the pore pressure field in the poroelastic domain $p_{\mathrm{M}}(\mathbf{x},t) : \Omega_{\mathrm{M}} \times \mathbb{R}^+ \to \mathbb{R}$, and the fluid pressure in the fracture domain $p_{\mathrm{F}}(\mathbf{x},t) : \Gamma_{\mathrm{F}} \times \mathbb{R}^+ \to \mathbb{R}$ for the system

$$
\begin{aligned}
-\boldsymbol{\sigma}(\boldsymbol{\varepsilon}[\mathbf{u}], p_{\mathrm{M}}) \cdot \boldsymbol{\nabla} &= \mathbf{0} && \text{in } \Omega_{\mathrm{M}} \times (0,T], && \text{(3.4a)}\\
\mathbf{u} &= \mathbf{u}^{\mathrm{p}} && \text{on } \Gamma_{\mathrm{M,D}}^{(u)} \times (0,T], && \text{(3.4b)}\\
\mathbf{t} := \boldsymbol{\sigma} \cdot \mathbf{n} &= \mathbf{t}^{\mathrm{p}} && \text{on } \Gamma_{\mathrm{M,N}}^{(u)} \times (0,T], && \text{(3.4c)}\\
\boldsymbol{\sigma} \cdot \mathbf{n} + p_{\mathrm{F}}\, \mathbf{n} &= 0 && \text{on } \Gamma_{\mathrm{F}} \times (0,T], && \text{(3.4d)}\\
\dot{\Phi}_{\mathrm{M}}(\boldsymbol{\varepsilon}[\mathbf{u}], p_{\mathrm{M}}) + \mathbf{w}_{\mathrm{M}}(\boldsymbol{\zeta}[p_{\mathrm{M}}]) \cdot \boldsymbol{\nabla} &= 0 && \text{in } \Omega_{\mathrm{M}} \times (0,T], && \text{(3.4e)}\\
p_{\mathrm{M}} &= p^{\mathrm{p}} && \text{on } \Gamma_{\mathrm{M,D}}^{(p)} \times (0,T], && \text{(3.4f)}\\
w_{\mathrm{M}} := \mathbf{w}_{\mathrm{M}} \cdot \mathbf{n} &= w^{\mathrm{p}} && \text{on } \Gamma_{\mathrm{M,N}}^{(p)} \times (0,T], && \text{(3.4g)}\\
[\![\mathbf{w}_{\mathrm{M}}]\!]_{\mathrm{F}} \cdot \mathbf{n}_{\mathrm{F}} + q_{\mathrm{L}} &= 0 && \text{on } \Gamma_{\mathrm{F}} \times (0,T], && \text{(3.4h)}\\
\dot{\Phi}_{\mathrm{F}}(\mathbf{u}, p_{\mathrm{F}}) + \mathbf{w}_{\mathrm{F}}(\boldsymbol{\zeta}_{\mathrm{F}}[p_{\mathrm{F}}]) \cdot \boldsymbol{\nabla}_{\mathrm{F}} + \frac{q_{\mathrm{L}}}{\tau} &= 0 && \text{in } \Gamma_{\mathrm{F}_i} \times (0,T], && \text{(3.4i)}\\
p_{\mathrm{F}} &= p^{\mathrm{p}} && \text{on } \mathcal{L}_{\mathrm{F}_i,\mathrm{D}} \times (0,T], && \text{(3.4j)}\\
w_{\mathrm{F}} := \mathbf{w}_{\mathrm{F}} \cdot \mathbf{n} &= w^{\mathrm{p}} && \text{on } \mathcal{L}_{\mathrm{F}_i,\mathrm{N}} \times (0,T], && \text{(3.4k)}\\
\sum_{j=1}^{n_{\mathrm{F}}} \mathbf{w}_{\mathrm{F}} \cdot \mathbf{n}|_{\Gamma_{\mathrm{F}_j}} &= 0 && \text{at } \cap_{j=1}^{n_{\mathrm{F}}} \Gamma_{\mathrm{F}_j} \times (0,T], && \text{(3.4l)}
\end{aligned}
$$

together with the initial conditions

$$
\begin{aligned}
\Phi_{\mathrm{M}} &= \Phi_{\mathrm{M}}^{\mathrm{p}} && \text{on } \Omega_{\mathrm{M}} \text{ at } t = 0, && \text{(3.5a)}\\
\Phi_{\mathrm{F}} &= \Phi_{\mathrm{F}}^{\mathrm{p}} && \text{on } \Gamma_{\mathrm{F}} \text{ at } t = 0. && \text{(3.5b)}
\end{aligned}
$$

The introduced vector $\mathbf{n}_{\mathrm{F}}$ is defined as the vector normal to the fracture, $\mathcal{L}_{\mathrm{F}_i}$ is the exterior boundary of the fractures, $[\![\bullet]\!]_{\mathrm{F}}$ is the jump of a quantity across the fracture and the constitutive relation for the fluid velocity in the fracture is given as

$$
\mathbf{w}_{\mathrm{F}}(\boldsymbol{\zeta}_{\mathrm{F}}[p_{\mathrm{F}}]) := -\mathbf{K}_{\mathrm{F}} \cdot \boldsymbol{\zeta}_{\mathrm{F}}[p_{\mathrm{F}}], \qquad \boldsymbol{\zeta}_{\mathrm{F}}[p_{\mathrm{F}}] := \boldsymbol{\nabla}_{\mathrm{F}} p_{\mathrm{F}} = [\mathbf{I} - \mathbf{n}_{\mathrm{F}} \otimes \mathbf{n}_{\mathrm{F}}] \cdot \boldsymbol{\nabla} p_{\mathrm{F}}, \qquad (3.6)
$$

with the permeability tensor $\mathbf{K}_{\mathrm{F}}{=}(\tau^2/12\eta)\mathbf{I}$ for the case of isotropy. The fluid velocity and storage function of the matrix are given in (2.47) and (2.49).

The storage function for the fluid in the fracture domain is given as

$$\Phi_{\mathrm{F}}(\mathbf{u}, p_{\mathrm{F}}) := 1 + e_{\mathrm{F}} + \frac{p_{\mathrm{F}}}{K^f}, \tag{3.7}$$

where the interaction between the fractures and the matrix is defined by the volumetric strain in the fracture and the leak-off of fluid from the fracture into the rock is introduced as q_{L}. Finally, the pressure field is assumed to be continuous.
With this modeling approach it is i.a. possible to analyze the different fluid-flow mechanisms on the meso-scale as studied in detail in [78]. This is shown in Fig. 3.3 b) by means of the inverse quality factor obtained for a 2-dimensional box of poroelastic medium including two perpendicular fractures with an initial high aspect ratio $2a/\tau = 1\mathtt{e}{+}4$. The seismic attenuation caused mainly by fracture flow on the meso-scale leads to the highest peak. Additionally, the critical frequency is high for this case. These effects are caused by the high hydraulic conductivity of the fractures, allowing for a faster fluid flow process. An excitation of the setup e.g. in vertical direction leads to a fluid flow from the horizontal fracture to the vertical fracture. This is caused by the strong deformation of the horizontal fracture resulting in a high pressure gradient in the fracture network. The results focusing on the fracture flow could be obtained by setting the permeability of the matrix extremely low to account for an impermeable surrounding matrix domain. Then, the fluid flow is mainly located within the fracture. The second fluid flow mechanism, in form of leak-off, leads to a low attenuation peak and a lower critical frequency as also visible in Fig. 3.2 b). This is caused by the deformation of the solid skeleton leading to solid-fluid interaction. Due to a high permeability of the surrounding matrix and fractures with constant fracture aperture, the fluid flows towards the porous rock. This process is slower than the fluid flow with in the fractures due to the lower conductivity of the matrix. The third attenuation that is presented in the figure shows two attenuation peaks, referring to the two main fluid flow mechanisms. When both processes occur during the simulation, the leak-off is slightly faster leading to a slightly larger critical frequency than for the pure leak-off effect. The fracture flow dominates the processes leading to a significant higher attenuation peak. This second peak of the attenuation overlaps with the attenuation mainly caused by flow within the fractures.
The main advantage of the modeling of meso-scale fractures in porous rock using the sharp interface formulation is the possibility to investigate fractures independent of their fracture aperture. This is an important issue as it can be shown, that attenuation caused by wave-induced fluid flow increases with decreasing fracture aperture as well as the coupling effects that get stronger. Another advantage is that the degrees of freedom can be reduced, as the fractures do not need to be meshed in full dimension. This is possible due to the assumption of dimensional reduction, i.e. the assumption that the fluid flow in the fractures is modeled as a 1-dimensional (2-dimensional) process in a 2-dimensional (3-dimensional) poroelastic matrix. Though, the modeling of more complex fracture networks, especially in 3-dimensional, is limited by the numbers of degrees of freedom that occur for meshing the surrounding matrix.

Diffuse interface formulation: One of the numerical models accounting for fractures in fluid-saturated porous media, that has gained importance in literature, is the phase field formulation. This theory provides a useful formulation for the application to fracture problems. The phase field approach for brittle fracture is studied in literature, see e.g. [34, 46, 73]. The combination of the phase field formulation for fractures with a poroelastic formulation for the background, provides several advantages in comparison with the introduced approaches to capture the hydro-mechanical processes in fractured porous media. The application of the phase field method to fracture problems in porous media is recently discussed in several studies [17, 25, 44, 45, 47, 48]. In these investigations the focus lies on the numerical modeling of fracture propagation in porous or poroelastic media and the qualitative description of the coupling mechanisms. The key feature of this approach is that the fractures are assigned to a scalar damage variable to describe them in a diffuse fashion, embedded in a poroelastic matrix with side length L as shown in Fig. 3.4 a) for two perpendicular fractures in a 2-dimensional setup. Along the fractures, the damage variable is chosen d=1 whilst d=0 refers to the undamaged state.

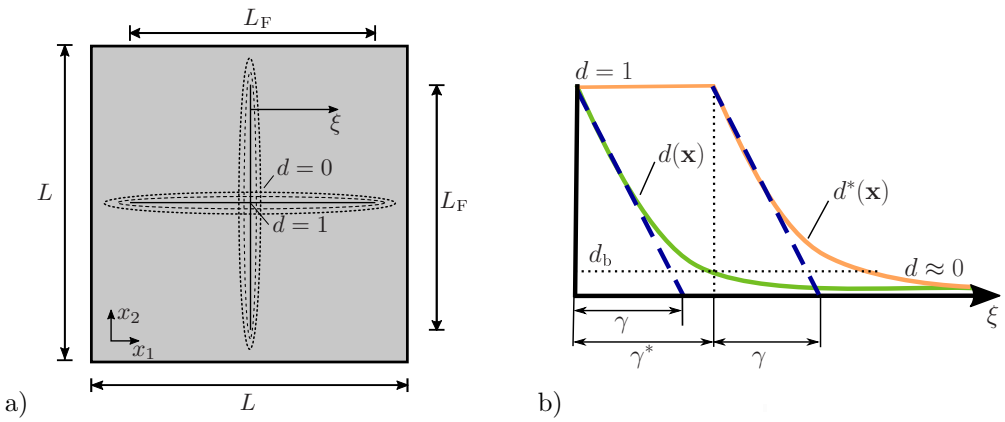

Figure 3.4: *Diffuse interface model. a) control volume with two intersecting fractures b) Damage field along one fracture. Here d^* refers to the modified damage field and d is the standard diffuse damage field. [56]*

The approach is based on the implementation of [44, 45, 48], where the local equations are the balance of fluid mass and balance of linear momentum with related constitutive relations for the stress, the fluid pressure and the fluid flow. The diffuse interface formulation is coupled to the **u**-p-formulation, which is the basis for the investigated studies of porous media. Miehe et al. [44] propose an anisotropic stress concept by introducing the decomposition of strains. This is introduced to account for crack opening and closing, i.e. different behavior under tension or compression. In this thesis, the focus is set on seismic stimulation of fracture networks with very low excitation amplitudes.
Having these assumptions in mind, the standard **u**-p-formulation given in (2.48) is changed to a coupled system, where the model variables are the damage field $d(\mathbf{x}, t) : \Omega \times \mathbb{R}^+ \rightarrow [0, 1]$, the displacement field $\mathbf{u}(\mathbf{x}, t) : \Omega \times \mathbb{R}^+ \rightarrow \mathbb{R}^3$, and the pore pressure $p(\mathbf{x}, t) : \Omega \times \mathbb{R}^+ \rightarrow \mathbb{R}$.

The system is defined as

$$\Theta(d, \boldsymbol{\varepsilon}[\mathbf{u}], p) - D(\dot{d}) + \mathbf{f}(\boldsymbol{\zeta}[d]) \cdot \boldsymbol{\nabla} = \mathbf{0} \quad \text{in } \Omega \times (0,T], \tag{3.8a}$$

$$d = 1 \quad \text{on } \Gamma_{\mathrm{F}} \times (0,T], \tag{3.8b}$$

$$d = d^{\mathrm{p}} \quad \text{on } \Gamma_{\mathrm{D}}^{(p)} \times (0,T], \tag{3.8c}$$

$$f := \mathbf{f} \cdot \mathbf{n} = f^{\mathrm{d}} \quad \text{on } \Gamma_{\mathrm{N}}^{(d)} \times (0,T], \tag{3.8d}$$

$$-\boldsymbol{\sigma}(d, \boldsymbol{\varepsilon}[\mathbf{u}], p) \cdot \boldsymbol{\nabla} = \mathbf{0} \quad \text{in } \Omega \times (0,T], \tag{3.8e}$$

$$\mathbf{u} = \mathbf{u}^{\mathrm{p}} \quad \text{on } \Gamma_{\mathrm{D}}^{(u)} \times (0,T], \tag{3.8f}$$

$$\mathbf{t} := \boldsymbol{\sigma} \cdot \mathbf{n} = \mathbf{t}^{\mathrm{p}} \quad \text{on } \Gamma_{\mathrm{N}}^{(u)} \times (0,T], \tag{3.8g}$$

$$\dot{\Phi}(d, \boldsymbol{\varepsilon}[\mathbf{u}], p) + \mathbf{w}(\boldsymbol{\zeta}[p]) \cdot \boldsymbol{\nabla} = \mathbf{0} \quad \text{in } \Omega \times (0,T], \tag{3.8h}$$

$$p = p^{\mathrm{p}} \quad \text{on } \Gamma_{\mathrm{D}}^{(p)} \times (0,T], \tag{3.8i}$$

$$w := \mathbf{w} \cdot \mathbf{n} = w^{\mathrm{p}} \quad \text{on } \Gamma_{\mathrm{N}}^{(p)} \times (0,T]. \tag{3.8j}$$

This thesis restricts on a quantitative analysis of the hydro-mechanical coupling in the diffuse interface model. Additionally, stationary fractures with prescribed "interior" boundary conditions are considered. The viscous regularization $D(\dot{d})$ including Griffith's criterion is considered for propagating fractures and is therefore neglected in this thesis. Additionally, the constitutive relations for the damage flux $\mathbf{f}$ and the damage source term are simplified and introduced as

$$\mathbf{f}(\boldsymbol{\zeta}[d]) := -\gamma^2 \boldsymbol{\zeta}[d], \quad \boldsymbol{\zeta}[d] := \boldsymbol{\nabla} d, \tag{3.9a}$$

$$\Theta(d, \boldsymbol{\varepsilon}[\mathbf{u}], p) = \Theta(d) := d. \tag{3.9b}$$

The storage function and seepage velocity are given in (2.47) and (2.49), respectively. The porosity and permeability in the diffuse fracture field are defined via a mixture rule that is given in detail in paper C. This definitions lead to a decoupling of the damage conservation law (3.8a) from the equation system accounting for poroelasticity, i.e. (3.8h) and (3.8e). Thus, the damage field can be derived a priori and the resulting damage distribution $d(\mathbf{x})$ serves as an input parameter for the problem solved by $\mathbf{u}$-p-formulation. The constitutive relation for the stress is, contrary to the standard formulation in (2.40), given as

$$\boldsymbol{\sigma}(\boldsymbol{\varepsilon}[\mathbf{u}], p) := a(d)\mathbb{E} \colon \boldsymbol{\varepsilon} - \alpha(d) p \mathbf{I}, \quad \boldsymbol{\varepsilon}[\mathbf{u}] := (\mathbf{u} \otimes \boldsymbol{\nabla})^{\mathrm{sym}}. \tag{3.10}$$

Here, a degradation function $a(d)$ is applied on the material stress of the solid phase of the poroelastic medium. It is defined as

$$a(d) = (1-\kappa)(1-d)^2 + \kappa, \quad 0 < \kappa \ll 1. \tag{3.11}$$

For numerical stability, the small parameter κ is chosen as introduced in [47]. Paper C proposes the investigation of this degradation function depending on a novel definition of a modified damage variable d^* defined as

$$d^* = \begin{cases} 1, & d \geq d_{\mathrm{b}}, \\ \frac{d}{d_{\mathrm{b}}}, & d < d_{\mathrm{b}}, \end{cases} \tag{3.12}$$

where d_b is a threshold value derived by the evaluation of the analytical solution for one single fracture. Here,

$$d_b = \exp\left(-\frac{\gamma^*}{\gamma}\right). \tag{3.13}$$

Thus, the degradation function is reformulated by

$$a(d^*) \quad = \quad (1-\kappa)(1-d^*)^2 + \kappa, \quad 0 < \kappa \ll 1. \tag{3.14}$$

This degradation function is assumed to act on the Biot-Willis-coefficient α in the form $\alpha = 1 - a(d)\, K/K^\mathrm{S}$. This is a logical choice when assuming a degradation of the solid phase of the medium.

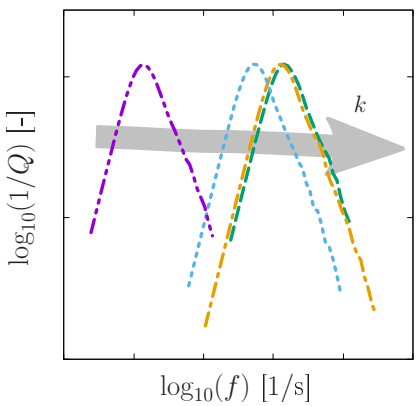

Figure 3.5: *Attenuation of a domain containing two perpendicular fractures, for varying permeability of the damage zone k of the control volume given by a mixture rule [56].*

Taking into account this system of equations, meso-scale heterogeneities in form of fractures in porous rock can be studied by means of the attenuation as shown exemplary in Fig. 3.5 for varying permeability of the damage zone. The typical curve including the low- and high-frequency domain as well as the attenuation peak is presented. The variation of the permeability in the damage zone is derived following the mixture rule ranging between the permeability of the surrounding matrix (d=0) and the higher fracture permeability (at d=1) given in detail in paper C. In the example it ranges between the harmonic and the arithmetic mean, which causes a shift of the attenuation in frequency. The attenuation peak remains at the same height, due to the underlying geometry (fracture aperture τ=1e-5 m) that is the same for all examples. Meaning that the same geometry of two perpendicular intersecting fractures with the same damage distribution $d(\mathbf{x})$ is used for the calculations associated to the results in Fig. 3.5 applying the modified damage variable d^*. It can be seen that the effect of the lower permeable surrounding rock matrix gets stronger for the harmonic mean of the mixture rule for the permeability resulting in a lower frequency range of the associated attenuation. And vice versa, the attenuation is

dominated by the higher permeability of the fracture for the arithmetic mean, which leads to a faster process, i.e. a higher frequency range of the solution.
A major advantage of the diffuse interface formulation is the straight forward implementation. That is, the fractures can simply be attached a damage variable and the fracture network can be derived a priori as a stationary damage field formulation. Additionally, the damage field can directly be combined with Biot's equations of consolidation and provides the possibility to be extended straightforward with Griffith's theory to account for fracture growth. It is shown in paper C, that the method using the conventional damage variable d does not converge to the reference solution (the sharp interface model). This is mainly caused by the volumetric strain in the damage zone which is concentrated in one single element. This problem can be overcome by applying the modified damage variable d^*, that is constant near to the interface resulting in a volumetric strain that is no longer concentrated in one single element as introduced in paper C. Taking into account this modification, the diffuse interface model is valuable, i.e. converges towards the reference solution. The diffuse interface formulation is applicable for high aspect ratio fractures and provides a simple implementation of interacting fractures. Nevertheless, a more complex structure would lead to high numerical costs, caused by the high resolution of the damage zone that is needed to achieve quantitative valuable solutions.

3.3 Uncoupled diffusion in porous media

A special case occurs for an uncoupled diffusion equation. One example of an uncoupled system was e.g. introduced by Terzaghi [74, 75] for 1-dimensional consolidation. In this case Biot's equation can be decoupled resulting in an uncoupled diffusion equation for the pressure with a specific consolidation coefficient. In this thesis, however, the case of an uncoupled diffusion equation is solved for the diffusion of chloride ions in porous concrete. The motivation for this is, that the uncoupled diffusion equation can be solved for 3-dimensional models. The study is of particular interest for construction engineers, e.g. in the application for buildings (such as bridges) made from reinforced concrete. Here, the chloride ions react with the steel causing corrosion which affects the stability of the whole structure. Previous research findings into transport processes in concrete have revealed that the transport of chloride ions is one of the most important mechanisms in reinforced concrete and that meso-scale models are an appropriate tool to study the influence of heterogeneities on the effective properties of homogeneous macro-scale concrete [80, 84, 87]. With this assumption, the system of equations for porous media introduced in Chapter 2 can be reduced towards an uncoupled diffusion equation and solved under static conditions. In this approach, the field variable is the concentration c rather than the pressure in the investigation concerning natural porous media such as rock. The resulting equation of stationary mass diffusion is studied in detail in paper D.
On the meso-scale, porous concrete is modeled as a three phase material and an example of such a structure is given in Fig. 3.6 a). It consists of cement paste as background material, aggregates and an Interfacial Transition Zone (ITZ). The ITZ is a thin layer surrounding the aggregates that exhibits a much higher porosity and higher diffusivity compared to the cement paste. It can be explained to be formed due to a "wall" effect of

packing of cement paste against the aggregates as described in detail in [71]. The ITZ has a high effect on the overall material behavior of concrete. A large and growing body of literature has investigated the ITZ and its thickness, which is found to lie in the range of 0 to 50 μm possibly depending on the aggregate size [8, 21, 35, 51, 71, 85, 86]. A possible approach to numerical model the ITZ is the application of the diffuse interface formulation discussed before. In fact, it is under discussion in literature e.g. [51], that the porosity of the ITZ varies with a gradient, i.e. it is highest at the surface of the aggregates and gets lower in direction to the cement paste. This effect could simply be captured with the application of the phase field method, though the required high resolution of the zone would be numerically cost intensive as is determined in Section 3.2. It was shown that the smoothing length and relating thereto the size of the elements near the interface has to be chosen very small to obtain quantitatively valuable solutions. In this thesis, the model assumes an average permeability of the ITZ, which allows the modeling of the ITZ as an interface at the surface of the aggregates.

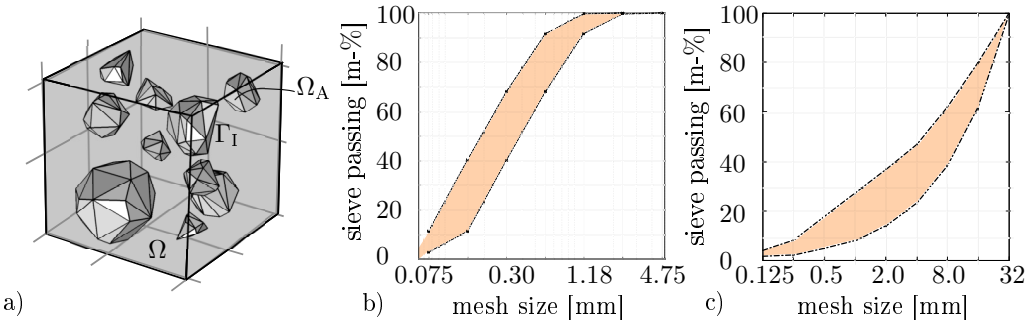

Figure 3.6: *a) Three-phase concrete. b) mixture based on ASTM Type I Portland cement with sand and water. c) Fuller's curve of aggregate mixture. [57].*

Taking into account these assumptions, a system of equations is established subsequently. The goal is to find the mass concentration of ions in the matrix $c_{\mathrm{M}} : \Omega_{\mathrm{M}} \times \mathbb{R}^+ \to \mathbb{R}$ and the mass concentration of ions in the ITZ $c_{\mathrm{I}} : \Gamma_{\mathrm{I}} \times \mathbb{R}^+ \to \mathbb{R}$ that solve the system

$$\mathbf{J}[c_{\mathrm{M}}] \cdot \boldsymbol{\nabla} = \mathbf{0} \qquad \text{in } \Omega_{\mathrm{M}}, \tag{3.15a}$$

$$c_{\mathrm{M}} = c^{\mathrm{P}} \qquad \text{on } \Gamma_{\mathrm{M,D}}, \tag{3.15b}$$

$$J := \mathbf{J}[c_{\mathrm{M}}] \cdot \mathbf{n} = J^{\mathrm{P}} \qquad \text{on } \Gamma_{\mathrm{M,N}}, \tag{3.15c}$$

$$\mathbf{J}_{\mathrm{T}}[c_{\mathrm{I}}] \cdot \boldsymbol{\nabla}_{\mathrm{T}} + \mathbf{J}[c_{\mathrm{M}}] \cdot \mathbf{n} = 0 \qquad \text{on } \Gamma_{\mathrm{I}}, \tag{3.15d}$$

$$c_{\mathrm{I}} = c_{\mathrm{I}}^{\mathrm{P}} \qquad \text{on } \mathcal{L}_{\mathrm{I,D}}, \tag{3.15e}$$

$$\mathbf{J}_{\mathrm{T}}[c_{\mathrm{I}}] \cdot \mathbf{n} = J_{\mathrm{T}}^{\mathrm{P}} \qquad \text{on } \mathcal{L}_{\mathrm{I,N}}. \tag{3.15f}$$

The constitutive relations are

$$\mathbf{J}[c] := -\mathbf{D} \cdot \boldsymbol{\zeta}[c], \quad \boldsymbol{\zeta}[c] := \boldsymbol{\nabla} c, \tag{3.16a}$$

$$\mathbf{J}_{\mathrm{T}}[c] := -\hat{\mathbf{D}}_{\mathrm{I}} \cdot \boldsymbol{\zeta}_{\mathrm{T}}[c], \quad \boldsymbol{\zeta}_{\mathrm{T}}[c] := \boldsymbol{\nabla}_{\mathrm{T}} c, \tag{3.16b}$$

where continuity of the concentration is applied ($c{=}c_{\mathrm{M}}{=}c_{\mathrm{I}}$ on Γ_{I}) and the tangential gradient operator that is derived on Γ_{I} is defined as $\boldsymbol{\zeta}_{\mathrm{T}}[c]{=}[\mathbf{I}-\mathbf{n}\otimes\mathbf{n}]\cdot\boldsymbol{\zeta}[c]$. The diffusivity tensor $\mathbf{D}$ [cm^2/s] and $\hat{\mathbf{D}}$ [cm^3/s] are, in case of isotropy, defined as

$$\mathbf{D} = D_{\mathrm{M}}\,\mathbf{I}, \quad \hat{\mathbf{D}}_{\mathrm{I}} = \hat{D}_{\mathrm{I}}\,\mathbf{I}, \tag{3.17}$$

where D_{M} is the diffusivity of the matrix and $\hat{D}_{\mathrm{I}}{=}f\cdot D_{\mathrm{CP}}$. Here, D_{CP} is the diffusivity of the pure cement paste and the factor f is introduced to describe the diffusivity of the ITZ efficiently as explained in detail in paper D. Prior studies have noted the importance of the shape of aggregates in concrete [8, 41] and, therefore, paper D proposes a procedure to generate the concrete structure. An important input parameter of the numerical models of concrete is the grading of concrete mixture that is given e.g. in form of sieve curves. In Fig. 3.6 b) and c) examples for sieve curves including the upper and lower bound are given for b) a mixture based on ASTM Type I Portland cement with sand and water [86] and c) for the common aggregate mixture given by Fuller's curve [84]. The mass of the aggregates is summed up and given in cumulative m-% versus the mesh size, i.e. the average diameter of the aggregates. The typical sieve curves provide a large range of sieve passing over length scales. This means, it includes a lot of very small and few very large aggregates. An explicit modeling of all these aggregates would lead to highly complex structures. The generation of such structures and especially the numercial simulation thereof is inaccessible at reasonable costs. Therefore, paper D proposes a novel procedure to handle the large range of aggregates given by the typical concrete mixtures, which is based on an analytical mixture rule. Thus, an efficient modeling of the mass diffusion in three-phase concrete is possible.

All approaches introduced in this Chapter account for heterogeneities on the meso-scale. It can be assumed that the diffusion is a local-phenomenon on the meso-scale which allows to derive effective properties on the macro-scale by computational homogenization which is introduced in detail in Chapter 4 by the example of a prototype, uncoupled, diffusion equation.

4 Variationally Consistent Homogenization

This Chapter introduces computational homogenization, based on first order homogenization, by means of a stationary and uncoupled diffusion equation as prototype for the introduced equations. For further information concerning the micro to macro scale transition, the interested reader is referred to [31, 32, 38, 39, 67].

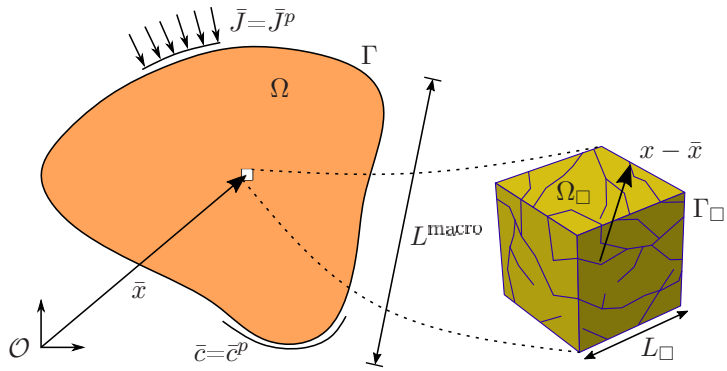

Figure 4.1: *Micro-to-macro transition. The fully resolved RVE represents one macroscopic material point in* Ω*.*

4.1 Preliminaries

Heterogeneities such as e.g. fractures in rock or aggregates in concrete strongly affect the macro-scale behavior of the porous material. The Direct Numerical Simulation of the particularized domain Ω is numerically extremely cost-intensive. Additionally, it is often not possible to obtain all details of the structure. Therefore, a macro-scale problem is introduced which depends on the micro-scale and is assumed to be homogeneous. The structural effects of the micro-scale are taken into account by applying computational homogenization. This method assumes two scales – micro- and macro-scale – of which the macro-scale refers to the large, observable scale (e.g. the reservoir) and the micro-scale is represented by the RVE problem.
The homogenization of micro-scale properties of porous media is based on the assumption that the length of the micro-scale RVE is much smaller than the characteristic length of the macro-scale problem, i.e. $L_\square \ll L^{\text{macro}}$, see Fig. 4.1). In standard homogenization a local boundary value problem is considered on the RVE, on which a macro-scale quantity is imposed by using corresponding boundary conditions.
In this thesis, the notation of the Variationally Consistent Homogenization (VCH) is used to derive the relevant scale transition relations. The VCH procedure consists of the following steps: First, the strong and weak form of the system of equations is derived from the fine-scale model, i.e. the reference model with full microscopic resolution in the

macro-scale domain Ω. Afterwards, the first-order homogenization is introduced in the spatial domain. Here, running averages are introduced, meaning that the domain Ω can be subdivided in domains $\Omega_\square$ (referred to as RVE). Then, averaging can be applied for these micro-domains that exist at each point of Ω. The macro-scale problem can then be stated under consideration of suitable boundary conditions on Γ. The idea is that, for sufficiently smooth problems, the "true" solution can be approximated by the two-scale model. To close the system, the micro-scale problem on a RVE has to be introduced.
In this thesis, the RVE-structures are created periodically to minimize boundary layer effects during VCH. The method is explained subsequently by means of a prototype diffusion problem. This serves as an example for the general application of the VCH concerning scale transition of a heterogeneous porous meso-scale towards a homogeneous macro-scale problem.

4.2 Fine-scale problem

The fine-scale problem refers to the detailed domain Ω with heterogeneous micro-structure, i.e. the fine-scale features are resolved for the entire problem. The strong formulation of an uncoupled mass diffusion equation in porous media is based on Fick's law [20]. The aim is to find, under static conditions, the concentration $c : \Omega \times \mathbb{R}^+ \to \mathbb{R}$ that solves the system

$$\mathbf{J}[c] \cdot \boldsymbol{\nabla} = \mathbf{0} \qquad \text{in } \Omega, \tag{4.1a}$$

$$c = c^{\mathrm{P}} \qquad \text{on } \Gamma_{\mathrm{D}}, \tag{4.1b}$$

$$\mathbf{J} \cdot \mathbf{n} = J^{\mathrm{P}} \qquad \text{on } \Gamma_{\mathrm{N}}. \tag{4.1c}$$

The constitutive relation for the mass flux $\mathbf{J}$ is defined as

$$\mathbf{J}[c] := -\mathbf{D} \cdot \boldsymbol{\zeta}[c], \qquad \boldsymbol{\zeta}[c] := \boldsymbol{\nabla} c, \tag{4.2}$$

where square brackets $\bullet[\diamond]$ relate to operational dependency of $\bullet$ on $\diamond$ and $\boldsymbol{\zeta}[c]$ is the gradient of the mass concentration c. The diffusivity tensor $\mathbf{D}$ is, in case of isotropy, defined as

$$\mathbf{D} = D\, \mathbf{I}, \tag{4.3}$$

where $D{=}D_{1,2,\ldots,n}$ in Ω for n phases with different diffusivity.
The weak form of this system of equations is obtained upon multiplying by the test function $\delta c \in \mathbb{C}^0$, applying the given boundary conditions and integrating by parts. Then the standard space-variational format for the system in (4.1) is introduced as follows: Find $c(\mathbf{x})$ in the suitable trial set $\mathbb{C}$ that solves

$$\int_\Omega \boldsymbol{\nabla} c \cdot \mathbf{D} \cdot \boldsymbol{\nabla} \delta c \, \mathrm{d}\Omega = -\int_{\Gamma_N} J^{\mathrm{P}} \delta c \, \mathrm{d}\Gamma \qquad \forall \delta c \in \mathbb{C}^0, \tag{4.4}$$

where $\mathbb{C}^0$ is the appropriately defined test space.

4.3 First-order homogenization in the spatial domain

Now the two-scale problem shall be defined, i.e. a micro-scale problem solved on $\Omega_\square$ and a macro-scale problem solved on Ω. To this end, a running average is introduced on the cubic domain $\Omega_\square$ which is located at each macro-scale point $\bar{\mathbf{x}} \in \Omega$. Therefore, the space-variational problem in (4.4) is replaced by finding $c(\mathbf{x}) \in \mathbb{C}_{\mathrm{FE}^2}$ that solves

$$\int_\Omega a_\square(c, \delta c)\, \mathrm{d}\Omega = -\int_{\Gamma_\mathrm{N}} J^\mathrm{P} \delta c\, \mathrm{d}\Gamma_\mathrm{N} \qquad \forall \delta c \in \mathbb{C}_{\mathrm{FE}^2}, \tag{4.5}$$

where the pertinent space-variational form is given as

$$a_\square(c, \delta c) \quad = \langle \boldsymbol{\nabla} c \cdot \mathbf{D} \cdot \boldsymbol{\nabla} \delta c \rangle_\square \,. \tag{4.6}$$

Here, the volume averaging operator is introduced as

$$\bar{\bullet} = \langle \bullet \rangle_\square = \frac{1}{|\Omega_\square|} \int_{\Omega_\square} \bullet \, \mathrm{d}\Omega, \tag{4.7}$$

The scale-separation is introduced via first-order homogenization, meaning that a macro-scale quantity is imposed on the micro-scale problem that varies linearly on a RVE. The micro-scale mass concentration c is decomposed into a macro-scale part c^M and a fluctuation part c^s within each RVE in the format

$$c = c^\mathrm{M}[\bar{c}] + c^\mathrm{s}, \quad \text{with} \quad c^\mathrm{M}(\mathbf{x}) := \bar{c} + \bar{\boldsymbol{\zeta}} \cdot (\mathbf{x} - \bar{\mathbf{x}}), \quad \bar{\boldsymbol{\zeta}} := \boldsymbol{\zeta}[\bar{c}]. \tag{4.8}$$

Note that $\bar{c}$ is the constant offset of the concentration field in the RVE. And, comparable to a rigid body mode, it doesn't contribute to the energy of the system. For convenience, it can be chosen $\bar{c}$=0. The two-scale trial and test spaces are defined as

$$\mathbb{C}_{\mathrm{FE}^2} := \{c|_{\Omega_{\square,\mathrm{j}}} = c^\mathrm{M}[\bar{c}] + c^\mathrm{s}_\mathrm{j},\ c^\mathrm{s}_\mathrm{j} \in \mathbb{C}^\mathrm{s}_{\square,\mathrm{j}},\ \bar{c} \in \bar{\mathbb{C}}\}, \tag{4.9a}$$

$$\mathbb{C}^0_{\mathrm{FE}^2} := \{\delta c|_{\Omega_{\square,\mathrm{j}}} = c^\mathrm{M}[\delta\bar{c}] + \delta c^\mathrm{s}_\mathrm{j},\ \delta c^\mathrm{s}_\mathrm{j} \in \mathbb{C}^\mathrm{s}_{\square,\mathrm{j}},\ \delta\bar{c} \in \bar{\mathbb{C}}^0\}, \tag{4.9b}$$

where $\bar{\mathbb{C}}$ and $\mathbb{C}^\mathrm{s}_{\square,\mathrm{j}}$ are the finite element discretized trial spaces for the macro- and micro-scale problem on $\Omega_{\square,\mathrm{j}}$. The trial space for the macro-scale problem is $\bar{\mathbb{C}}^0$. The assumption is applied that there exists a component c^s and corresponding space $\mathbb{C}^\mathrm{s}_{\square,\mathrm{j}}$ for each single RVE $\Omega_{\square,\mathrm{j}}$ in the form

$$c \in \mathbb{C}_{\mathrm{FE}^2} \rightarrow (\bar{c}, \{c^\mathrm{s}_\mathrm{j}\}) \in \bar{\mathbb{C}} \times [\mathsf{X}_\mathrm{j} \mathbb{C}^\mathrm{s}_{\square,\mathrm{j}}]. \tag{4.10}$$

The two-scale problem is restated, taking into account the interpretation $\delta c^\mathrm{s}_\mathrm{j} = \delta c^\mathrm{s}$ inside $\Omega_{\square,\mathrm{j}}$, by finding $(\bar{c}, \{c^\mathrm{s}_\mathrm{j}\}) \in \mathbb{C}_{\mathrm{FE}^2}$ that solves

$$\int_\Omega a_\square(c, c^\mathrm{M}[\delta\bar{c}] + \delta c^\mathrm{s})\, \mathrm{d}\Omega = -\int_{\Gamma_\mathrm{N}} J^\mathrm{P}[c^\mathrm{M}[\delta\bar{c}] + \delta c^\mathrm{s}]\, \mathrm{d}\Gamma \qquad \forall \delta c \in \mathbb{C}^0_{\mathrm{FE}^2}. \tag{4.11}$$

4.4 Macro-scale problem

Now, only macroscopic contributions to the test functions are considered, i.e. $\delta c^{\mathrm{s}} = 0$. As a result, the homogenized macro-scale problem from (4.11) can be obtained as that of finding $\bar{c} \in \bar{\mathbb{C}}$ such that

$$-\int_{\Omega} \bar{\mathbf{J}} \cdot [\boldsymbol{\nabla} \delta \bar{c}] \mathrm{d}\Omega = -\int_{\Gamma_n} \bar{J}^{\mathrm{P}} \delta \bar{c} \, \mathrm{d}\Gamma \qquad \forall \delta \bar{c} \in \bar{\mathbb{C}}^0, \tag{4.12}$$

where $\bar{J}^{\mathrm{P}}$ is defined as the suitably homogenized quantity on the Neumann boundary. The macro-scale flux is defined as

$$\bar{\mathbf{J}} := \langle \mathbf{J} \rangle_{\square} = \langle -\mathbf{D} \cdot \boldsymbol{\zeta}[c] \rangle_{\square} \, . \tag{4.13}$$

Here the transition of the volume average of the mass flux into the surface integral can be introduced as

$$\bar{\mathbf{J}} = \frac{1}{|\Omega_{\square}|} \int_{\Gamma_{\square}} J \, [\mathbf{x} - \bar{\mathbf{x}}] \, \mathrm{d}\Gamma, \tag{4.14}$$

where $J{:=}\mathbf{J} \cdot \mathbf{n}$ is the boundary flux.
Clearly, the homogenized flux depends on c. In the subsequent section, the RVE-problem is introduced, such that

$$\bar{\mathbf{J}} = \bar{\mathbf{J}}\{\bar{\boldsymbol{\zeta}}\}, \tag{4.15}$$

i.e., $\bar{\mathbf{J}}$ is implicitly depending on the homogenized field.[1] This is exactly the relation needed to solve (4.12).

4.5 Micro-scale problem on an RVE

After having defined the macro-scale problem, the micro-scale problem on an RVE is introduced subsequently. The concentration is decomposed as introduced in (4.8) in the macro-scale part c^{M} and a fluctuation part c^{s}. The fluctuation part is assumed to be periodic on $\Omega_{\square}$ such that

$$[\![c^{\mathrm{s}}]\!]_{\square} = 0 \quad \forall \mathbf{x} \in \Gamma_{\square}^{+}. \tag{4.16}$$

Here, the difference operator $[\![\bullet]\!]_{\square}(\mathbf{x}) = \bullet(\mathbf{x}^{+}) - \bullet(\mathbf{x}^{-})$ is introduced, where $\mathbf{x} \in \Gamma_{\square}^{+}$ are the image points and $\mathbf{x} \in \Gamma_{\square}^{-}$ the corresponding mirror points as shown in Fig. 4.2.
This micro-periodicity is applied in a variational form, i.e.

$$d_{\square}(\delta\lambda, c) \quad = d_{\square}(\delta\lambda, \bar{\boldsymbol{\zeta}} \cdot \mathbf{x}), \quad \forall \delta\lambda \in \mathbb{T}_{\square}. \tag{4.17}$$

[1] Here, due to the invariance at a constant value, $\bar{\mathbf{J}}$ will not depend on $\bar{c}$, but only on its gradient, for this linear model problem.

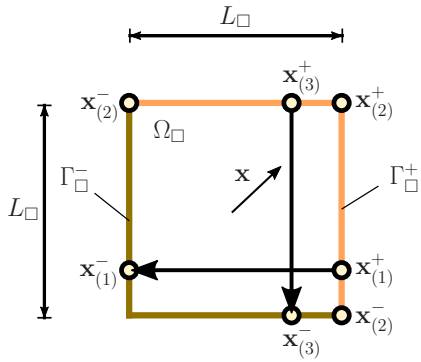

Figure 4.2: *RVE $\Omega_\square$ with the decomposition of the boundary $\Gamma_\square$ into image and mirror boundaries $\Gamma^+_\square$ and $\Gamma^-_\square$.*

Here, the RVE forms are defined as

$$d_\square(\lambda, c) := \frac{1}{|\Omega_\square|} \int_{\Gamma^+_\square} \lambda [\![c]\!]_\square \, \mathrm{d}\Gamma, \tag{4.18a}$$

$$d_\square(\lambda, \bar{\boldsymbol{\zeta}} \cdot \mathbf{x}) := \frac{1}{|\Omega_\square|} \int_{\Gamma^+_\square} \lambda [\![\mathbf{x}]\!]_\square \, \mathrm{d}\Gamma \cdot \bar{\boldsymbol{\zeta}}, \tag{4.18b}$$

where λ is a Lagrange multiplier that can be interpreted as a boundary flux on $\Gamma^+_\square$. The space for λ is defined as

$$\mathbb{T}_\square = [\mathrm{L}_2(\Gamma^+_\square)]^3 \tag{4.19}$$

with L_2 denoting the space of square integrable functions. Thus, the space-variational RVE format is stated as follows: For a given gradient $\bar{\boldsymbol{\zeta}}$ find $c(\mathbf{x}) \in \mathbb{C}^{\mathrm{s}}_\square, \lambda \in \mathbb{T}_\square$ that solves

$$a_\square(c, \delta c) - d_\square(\lambda, \delta c) = 0, \qquad \forall \delta c \in \mathbb{C}^{\mathrm{s}}_\square, \tag{4.20a}$$

$$- d_\square(\delta\lambda, c) = -d_\square(\delta\lambda, \bar{\boldsymbol{\zeta}} \cdot \mathbf{x}), \qquad \forall \delta\lambda \in \mathbb{T}_\square. \tag{4.20b}$$

From the solution of (4.20 a, b) the homogenized flux $\bar{\mathbf{J}}$ may be computed. Hence, $\bar{\mathbf{J}}{=}\bar{\mathbf{J}}\{\bar{\boldsymbol{\zeta}}\}$ is derived by the RVE-problem and returned to the Macro-scale problem in (4.12).
It can be shown, that the Hill-Mandel macro-homogeneity condition [26, 27, 50] is fulfilled as a property built into the problem formulation of VCH. To prove the Hill-Mandel criterion, the necessary assumptions and mathematical steps are explained in the following.
First, the volume averaging rule for the concentration gradient $\boldsymbol{\zeta}$,

$$\langle \boldsymbol{\zeta}[c] \rangle = \bar{\boldsymbol{\zeta}}, \tag{4.21}$$

needs to be fulfilled. This is verified by considering the identity

$$\delta\bar{\mathbf{J}} \cdot \langle \boldsymbol{\zeta}[c] \rangle_\square = \frac{1}{|\Omega_\square|} \int_{\Gamma_{\square+}} (\delta\bar{\mathbf{J}} \cdot \mathbf{n}) \, c \, \mathrm{d}\Gamma = \frac{1}{|\Omega_\square|} \int_{\Gamma^+_\square} (\delta\bar{\mathbf{J}} \cdot \mathbf{n}) [\![\mathbf{x}]\!] \cdot \bar{\boldsymbol{\zeta}} \, \mathrm{d}\Gamma. = \delta\bar{\mathbf{J}} \cdot \bar{\boldsymbol{\zeta}}, \tag{4.22}$$

where Gauss' theorem was used in the first and last identity, and (4.20b) with $\delta\lambda{=}\delta\bar{\mathbf{J}}\cdot\mathbf{n}$ for a constant $\delta\bar{\mathbf{J}}$ gives the second identity.
Second, the Hill-Mandel macro-homogeneity for any two fields c' and c'' are solved for from (4.20 a,b) with $\bar{\boldsymbol{\zeta}}{=}\bar{\boldsymbol{\zeta}}'$ and $\bar{\boldsymbol{\zeta}}''$, respectively, must obey

$$\left\langle \mathbf{J}'\cdot\boldsymbol{\zeta}''\right\rangle_{\square} = \bar{\mathbf{J}}'\cdot\bar{\boldsymbol{\zeta}}''. \tag{4.23}$$

To prove this relation, it can be concluded that

$$\left\langle \mathbf{J}'\cdot\boldsymbol{\zeta}''\right\rangle_{\square} = a_{\square}(c',c'') = d_{\square}(\lambda',c'') = d_{\square}(\lambda',\bar{\boldsymbol{\zeta}}''\cdot\mathbf{x}) = \frac{1}{|\Omega_{\square}|}\int_{\Gamma^{+}_{\square}}\lambda'[\![\mathbf{x}]\!]\,\mathrm{d}\Gamma\cdot\bar{\boldsymbol{\zeta}}'', \tag{4.24}$$

where the second equality follows from (4.20a) with $\delta c{=}c''$ and the third equality follows from (4.20b) with $\delta\lambda{=}\lambda'$.
Finally, by choosing $\delta c{=}x_{\mathrm{i}}$ in (4.20b), the component-wise relation

$$\bar{J}'_{\mathrm{i}} = a_{\square}(c',x_{\mathrm{i}}) = d_{\square}(\lambda',x_{\mathrm{i}}) = \frac{1}{|\Omega_{\square}|}\int_{\Gamma^{+}_{\square}}\lambda'[\![x_{\mathrm{i}}]\!]\,\mathrm{d}\Gamma \tag{4.25}$$

can be obtained, which, inserted in (4.24) completes the proof.

5 Summary of appended papers

5.1 Paper A: Numerical Investigation of the Effective Skempton Coefficient in Porous Rock Containing Fluid-Filled Fracture Networks

Hydro-mechanics of fluid-filled fracture networks in porous rock is investigated. The paper, therefore, presents a numerical investigation of an effective Skempton coefficient for different setups. The Skempton coefficient measures the effect of changes in mean stress on the pore pressure under undrained conditions. It is analyzed in this paper by the use of numerical modeling to identify the limitations of common measurement setups in laboratory experiments. Therefore, the behavior of the numerically derived effective Skempton coefficient is compared to the pseudo-Skempton coefficient, which is known from laboratory measurements [53]. Throughout this study, the fluid-saturated rock is modeled as a poroelastic medium by applying Biot's theory in form of a displacement-pressure-formulation [2]. Using the scale separation explained in detail in chapter 1 and further, volume averaging techniques and computational homogenization are performed to analyze the material properties in time-, as well as frequency domain for the underlying setups. The paper presents at first a modified Cryer's problem consisting of a spherical sample embedded in a mantle, both treated as porous media with different material properties. Second the study provides stochastically generated fracture networks in a quadratic sample. The fractures are modeled as ellipses with moderate aspect ratio constituting highly porous inclusions in a more compact rock.
It was observed that the results of the local pressure measurement (i.e. the pseudo-Skempton coefficient) vary widely from the volume averaged properties (i.e. the effective Skempton coefficient). The investigation has revealed that the effective Skempton coefficient contains information about the sample and serves as a valuable quantity for the analysis of effective hydro-mechanical properties.

5.2 Paper B: Experimental determination of the Skempton coefficient: Challenges and opportunities

Pressure diffusion of pore fluid is numerically investigated to examine the crucial role of adequately designed laboratory measurements in the context of determining the Skempton coefficient. Here, the study takes up paper A with the goal to transfer the numerical results to experimental realizations.
The accurate measurement of the Skempton coefficient requires realization of undrained boundary conditions. But the implementation of this condition is challenging in experimental setups, where a dead volume always occurs due to the presence of tubes, sensors, connectors and many more. Therefore, the study analyzes the crucial role of this gauge

volume by using numerical investigations of pressure diffusion due to a volumetric loading of different samples. A detailed comparison is made between a homogeneous and a heterogeneous sample of fluid-saturated rock, modeled as spherical samples that are embedded in a mantle consisting of pore fluid and representing the dead volume. Thus, the study investigates a time-dependent boundary value problem combined with pressure-diffusion controlled flux of pore fluid for Biot's basic constitutive equations of linear poroelasticity [3]. The data obtained were evaluated using the ratio of the pseudo-Skempton coefficient introduced in paper A and [53] and the classic (elastic) Skempton coefficient solved for different ratios of storage capacities. The storage capacities of the samples were evaluated as the sum of corresponding volume and specific storage capacity, i.e. the change in fluid increment depending on the displacements of phases related to change in fluid pressure [64].
It was found that pressure diffusion influences the Skempton coefficient strongly depending on the storage capacity of the gauge volume. The paper has observed that valuable results of the Skempton coefficient can only be obtained if the characteristic time of the pressure diffusion has passed and for a small gauge volume, i.e. a volume order of magnitude smaller than the sample volume. These findings confirm the importance of thoroughly designed experimental setups and laboratory measurements.

5.3 Paper C: Diffuse interface modeling and Variationally Consistent Homogenization of fluid transport in fractured porous media

Pressure diffusion in a fractured poroelastic medium is investigated using a diffuse interface formulation to study how well the method accounts for the underlying hydro-mechanical coupling processes. The study, therefore, focuses on the sub-problem of hydro-mechanically triggered fluid transport in mechanically and hydraulically open, stationary fractures that are embedded in a poroelastic background medium. Within this framework the diffuse fracture phase field is analyzed in comparison with a sharp interface formulation of hydro-mechanically coupled fluid transport in fracture networks that serves as reference solution [31]. Both approaches take into account a poroelastic background medium described by a displacement-pressure formulation. The additional primary global fields are the fluid pressure in the fracture for the sharp interface method and the damage variable for the diffuse formulation. It is found within the scope of this study that the conventional fracture phase-field formulation fails in a suitable prediction of the fluid transport behavior. The paper therefore proposes a modification of the formulation by introducing a modified damage variable. These model formulations are analyzed numerically for two benchmark problems. First the outflux of fluid from a single drained fracture under compression is studied. Second, two perpendicular and intersecting fractures embedded in a poroelastic matrix are analyzed that serves as prototype RVEs for seismic attenuation in fluid-saturated fracture networks. The poroelastic RVEs are examined via up-scaling towards a viscoelastic large-scale model based on Variationally consistent Computational Homogenization.

It was observed that the conventional formulation does not converge towards the correct solution, whereas the modification leads to reasonable results and a very good approximation with the reference, if the smoothing length of the diffuse fracture is small. The findings showed that a high resolution of the fracture zone is required for quantitative results, even though the modified formulation was observed to be less sensitive for the finite element discretization.

5.4 Paper D: Modeling and computational homogenization of chloride diffusion in three-phase meso-scale concrete

Computational homogenization for modeling transport of chloride ions in porous concrete is introduced to investigate the effects of meso-scale heterogeneities in form of aggregate content and Interfacial Transition Zone (ITZ) on macro-scale properties. The concrete is modeled as a three-phase material consisting of the cement paste, the aggregates and the ITZ. The highly heterogeneous material is characterized by sieve analysis consisting of an aggregate mixture with a large range of aggregate sizes. Therefore, the paper develops modeling on different scales by combining numerical Variational Consistent Homogenization (VCH) with an analytical technique. The analytical assumptions are based on a mixture rule and account for lower, unresolved, length scales. Here, the properties of the unresolved length scales are determined a priori and homogenized to be included in the numerical modeling. The numerical models are generated using particle size distribution (PSD) for given sieve curves. At first a dense sphere packing is created based on the PSD. This information is used to generate a weighted Voronoi diagram, which is modified by a shrinking process to create artificial and periodic RVEs for the numerical investigations. The numerical investigations are compared with experimental results to validate the applied method. The overarching goal is to determine the impact of meso-scale heterogeneities on the effective diffusivity of a homogeneous macro-scale model.
It was found that the ITZ has a high impact on the macro-scale diffusivity of concrete. Additionally it could be shown that the numerically obtained results are in a good agreement with experimental studies. Assuming that the thickness of the ITZ is independent of aggregate size, allowed for accurate calibration of the model parameters. Additionally the different effects of aggregate size on the homogenized properties were emphasized.

6 Conclusions and Outlook

The main goal of this thesis is to elaborate a suitable toolbox to simulate transport processes in porous media. This has been developed for the multi-scale modeling of transport processes on the example of fluid flow in porous rock and transport of chloride ions in concrete. The hydro-mechanical effects of fractured meso-scale rock can be investigated by means of the presented approaches of coupling the behavior of fluid-filled fractures and the poroelastic material behavior of the surrounding rock. The interpretation of seismic attenuation provides a useful tool for reservoir characterization, as well as for the design and interpretation of experimental studies and points in the direction of studying fracture connectivity. The decoupling of the basic equations can be used to obtain reliable results for effective diffusivity of porous concrete, taking into account aggregate distributions and Interfacial Transition Zones.

The **main findings** are the following:

I) Meso-scale heterogeneities have a large effect on frequency-dependent macro-scale properties. In case of the examples studied in this thesis this means in particular, that the wave-induced fluid flow caused by pressure gradients in fractured meso-scale porous rock has a high influence on the seismic attenuation of a rock reservoir and that properties like the diffusivity of three-phase porous concrete affect the overall diffusivity of the macro-scale homogeneous model of concrete.

II) Numerical results can be transferred to experimental realizations. Here, in paper B the crucial role for accurate design of experimental studies is highlighted.

III) To obtain reliable macro-scale properties is not trivial and requires a suitable toolbox to capture the processes on multiple scales. An efficient and valuable modeling of fractures in porous rock with the introduced approaches showed individual limits and advantages, such as: 1) The reliable quantification of hydro-mechanical processes with the patchy saturation model but limitation of fracture geometry, studied in paper A and B, 2) The possibility of the sharp interface model to separate different flow mechanisms and to account for geological fractures but limitation to not too complex fracture networks and 3) The advantage of the diffuse interface formulation to capture complex fracture networks but limitation caused by the high resolution of fracture zone required for quantitative results, investigated in paper C. The derivation of macro-scale quantities of porous concrete, as analyzed in paper D, requires a valuable generation of meso-scale structures and a suitable modeling of all phases.

It is of interest for **future research** to investigate further aspects of the introduced models, e.g. the following:

I) The possibility to capture the hydro-mechanical coupling between fractures and porous rock with the diffuse interface formulation needs further insight, and a systematic analysis of more complex fracture networks and more permeable surrounding rock is recommended.

II) The combination of the mass diffusion in porous concrete also containing fractures is of interest for various research fields and would be interesting to consider with the proposed procedures.

III) An interesting problem is to embed the developed models into FE^2 type simulations. The FE^2 approach offers two possibilities. If the sub-scale relation is linear and static as discussed for diffusion in meso-scale concrete, the homogenization can be directly carried out in terms of a priori upscaling. If the sub-scale relation is nonlinear and/or transient, on the other hand, as in the considered case of fractured rock, the homogenization has to be done in a nested fashion. That means, the macro-scale and the meso-scale problem need to be derived in a coupled formulation, e.g. the macro-scale stresses depend on the effective strains derived from the meso-scale problem.

IV) A further field for future research is to enrich the discussed approaches with nonlinear material behavior such as non-Darcy type diffusion or viscoplastic models for the solid skeleton.

V) Possible further investigations include also to utilize the approaches in advanced calibration from experiments at different length scales.

References

[1] G. K. Batchelor. *An introduction to fluid dynamics*. Cambridge University Press, 2000.

[2] M. A. Biot. General theory of three-dimensional consolidation. *Journal of Applied Physics* **12**.2 (1941), 155–164.

[3] M. A. Biot. Mechanics of deformation and acoustic propagation in porous media. *Journal of Applied Physics* **33**.4 (1962), 1482–1498.

[4] S. Caré. Influence of aggregates on chloride diffusion coefficient into mortar. *Cement and Concrete Research* **33**.7 (2003), 1021–1028.

[5] P. Chadwick. *Continuum mechanics: Concise theory and problems*. Courier Corporation, 2012.

[6] M. Chapman, E. Liu, and X.-Y. Li. The influence of fluid sensitive dispersion and attenuation on AVO analysis. *Geophysical Journal International* **167**.1 (2006), 89–105.

[7] J. Charléty, N. Cuenot, L. Dorbath, C. Dorbath, H. Haessler, and M. Frogneux. Large earthquakes during hydraulic stimulations at the geothermal site of Soultz-sous-Forêts. *International Journal of Rock Mechanics and Mining Sciences* **44**.8 (2007), 1091–1105.

[8] H. Chen, Z. Zhu, L. Liu, W. Sun, and C. Miao. Aggregate shape effect on the overestimation of ITZ thickness: Quantitative analysis of Platonic particles. *Powder Technology* **289** (2016), 1–17.

[9] A. H.-D. Cheng. *Poroelasticity*. Springer, 2016.

[10] O. Coussy. *Poromechanics*. John Wiley & Sons, 2004.

[11] C. Cryer. A comparison of the three-dimensional consolidation theories of Biot and Terzaghi. *The Quarterly Journal of Mechanics and Applied Mathematics* **16**.4 (1963), 401–412.

[12] E. Detournay and A. H.-D. Cheng. "Fundamentals of poroelasticity". *Analysis and design methods*. Elsevier, 1993, pp. 113–171.

[13] S. Diamond and J. Huang. The ITZ in concrete–a different view based on image analysis and SEM observations. *Cement and Concrete Composites* **23**.2-3 (2001), 179–188.

[14] N. C. Dutta and H. Odé. Attenuation and dispersion of compressional waves in fluid-filled porous rocks with partial gas saturation (White model)—Part II: Results. *Geophysics* **44**.11 (1979), 1789–1805.

[15] N. C. Dutta and H. Odé. Attenuation and dispersion of compressional waves in fluid-filled porous rocks with partial gas saturation (White model)—Part II: Results. *Geophysics* **44**.11 (1979), 1789–1805.

[16] W. Ehlers. "Foundations of multiphasic and porous materials". *Porous media*. Springer, 2002, pp. 3–86.

[17] W. Ehlers and C. Luo. A phase-field approach embedded in the theory of porous media for the description of dynamic hydraulic fracturing. *Computer Methods in Applied Mechanics and Engineering* **315** (2017), 348–368.

[18] R. P. Ewing and B. Berkowitz. Stochastic pore-scale growth models of DNAPL migration in porous media. *Advances in Water Resources* **24**.3-4 (2001), 309–323.
[19] F. Feyel and J.-L. Chaboche. FE2 multiscale approach for modelling the elastoviscoplastic behaviour of long fibre SiC/Ti composite materials. *Computer Methods in Applied Mechanics and Engineering* **183**.3-4 (2000), 309–330.
[20] A. Fick. Ueber diffusion. *Annalen der Physik* **170**.1 (1855), 59–86.
[21] Y. Gao, G. De Schutter, G. Ye, Z. Tan, and K. Wu. The ITZ microstructure, thickness and porosity in blended cementitious composite: Effects of curing age, water to binder ratio and aggregate content. *Composites Part B: Engineering* **60** (2014), 1–13.
[22] M. G. Geers, V. G. Kouznetsova, and W. Brekelmans. Multi-scale computational homogenization: Trends and challenges. *Journal of Computational and Applied Mathematics* **234**.7 (2010), 2175–2182.
[23] R. Greve. *Kontinuumsmechanik: Ein Grundkurs für Ingenieure und Physiker*. Springer-Verlag, 2013.
[24] I. Gueven, P. Kurzeja, S. Luding, and H. Steeb. Experimental evaluation of phase velocities and tortuosity in fluid saturated highly porous media. *Proceedings in Applied Mathematics and Mechanics* **12**.1 (2012), 401–402.
[25] Y. Heider and B. Markert. A phase-field modeling approach of hydraulic fracture in saturated porous media. *Mechanics Research Communications* **80** (2017), 38–46.
[26] R. Hill. Elastic properties of reinforced solids: Some theoretical principles. *Journal of the Mechanics and Physics of Solids* **11**.5 (1963), 357–372.
[27] R. Hill. On constitutive macro-variables for heterogeneous solids at finite strain. *Proceedings of the Royal Society of London. A. Mathematical and Physical Sciences* **326**.1565 (1972), 131–147.
[28] O. Huseby, J. Thovert, and P. Adler. Geometry and topology of fracture systems. *Journal of Physics A: Mathematical and General* **30**.5 (1997), 1415.
[29] R. Jänicke. Computational homogenization and reduced order modeling of diffusion processes in fluid-saturated porous media. *Habilitationsschrift, Ruhr-Universität Bochum* (2015).
[30] R. Jänicke, S. Diebels, H.-G. Sehlhorst, and A. Düster. Two-scale modelling of micromorphic continua. *Continuum Mechanics and Thermodynamics* **21**.4 (2009), 297–315.
[31] R. Jänicke, B. Quintal, F. Larsson, and K. Runesson. Identification of viscoelastic properties from numerical model reduction of pressure diffusion in fluid-saturated porous rock with fractures. *Computational Mechanics* **63**.1 (2019), 49–67.
[32] R. Jänicke, B. Quintal, F. Larsson, and K. Runesson. Viscoelastic substitute models for seismic attenuation caused by squirt flow and fracture leak-off. *Geophysics* **84**.4 (2019), 1–39.
[33] R. Jänicke, B. Quintal, and H. Steeb. Numerical homogenization of mesoscopic loss in poroelastic media. *European Journal of Mechanics-A/Solids* **49** (2015), 382–395.
[34] M.-A. Keip, B. Kiefer, J. Schröder, and C. Linder. Special Issue on Phase Field Approaches to Fracture. *Computer Methods in Applied Mechanics and Engineering* **312** (2016), 1–2.

[35] D. Kong, T. Lei, J. Zheng, C. Ma, J. Jiang, and J. Jiang. Effect and mechanism of surface-coating pozzalanics materials around aggregate on properties and ITZ microstructure of recycled aggregate concrete. *Construction and Building Materials* **24**.5 (2010), 701–708.

[36] V. Kouznetsova, M. G. Geers, and W. M. Brekelmans. Multi-scale constitutive modelling of heterogeneous materials with a gradient-enhanced computational homogenization scheme. *International Journal for Numerical Methods in Engineering* **54**.8 (2002), 1235–1260.

[37] P. Kurzeja. *Waves in partially saturated porous media: An investigation on multiple scales*. Dissertationsschrift, Ruhr-Universität Bochum, Institut für Mechanik, 2013.

[38] F. Larsson, K. Runesson, and F. Su. Computational homogenization of uncoupled consolidation in micro-heterogeneous porous media. *International Journal for Numerical and Analytical Methods in Geomechanics* **34**.14 (2010), 1431–1458.

[39] F. Larsson, K. Runesson, and F. Su. Variationally consistent computational homogenization of transient heat flow. *International Journal for Numerical Methods in Engineering* **81**.13 (2010), 1659–1686.

[40] D. Law, J. Cairns, S. Millard, and J. Bungey. Measurement of loss of steel from reinforcing bars in concrete using linear polarisation resistance measurements. *NDT & E International* **37**.5 (2004), 381–388.

[41] L. Liu, D. Shen, H. Chen, and W. Xu. Aggregate shape effect on the diffusivity of mortar: A 3D numerical investigation by random packing models of ellipsoidal particles and of convex polyhedral particles. *Computers & structures* **144** (2014), 40–51.

[42] Y. J. Masson and S. R. Pride. Poroelastic finite difference modeling of seismic attenuation and dispersion due to mesoscopic-scale heterogeneity. *Journal of Geophysical Research: Solid Earth* **112**.B3 (2007).

[43] Y. J. Masson and S. R. Pride. Seismic attenuation due to patchy saturation. *Journal of Geophysical Research: Solid Earth* **116**.B3 (2011).

[44] C. Miehe and S. Mauthe. Phase field modeling of fracture in multi-physics problems. Part III. Crack driving forces in hydro-poro-elasticity and hydraulic fracturing of fluid-saturated porous media. *Computer Methods in Applied Mechanics and Engineering* **304** (2016), 619–655.

[45] C. Miehe, S. Mauthe, and S. Teichtmeister. Minimization principles for the coupled problem of Darcy–Biot-type fluid transport in porous media linked to phase field modeling of fracture. *Journal of the Mechanics and Physics of Solids* **82** (2015), 186–217.

[46] C. Miehe, F. Welschinger, and M. Hofacker. Thermodynamically consistent phase-field models of fracture: Variational principles and multi-field FE implementations. *International Journal for Numerical Methods in Engineering* **83**.10 (2010), 1273–1311.

[47] A. Mikelić, M. F. Wheeler, and T. Wick. Phase-field modeling of a fluid-driven fracture in a poroelastic medium. *Computational Geosciences* **19**.6 (2015), 1171–1195.

[48] A. Mikelić, M. F. Wheeler, and T. Wick. A phase-field method for propagating fluid-filled fractures coupled to a surrounding porous medium. *Multiscale Modeling & Simulation* **13**.1 (2015), 367–398.

[49] T. M. Müller, B. Gurevich, and M. Lebedev. Seismic wave attenuation and dispersion resulting from wave-induced flow in porous rocks—A review. *Geophysics* **75**.5 (2010), 75A147–75A164.

[50] S. Nemat-Nasser and M. Hori. *Micromechanics: Overall properties of heterogeneous materials*. Vol. 37. Elsevier, 2013.

[51] F. Nilenius, F. Larsson, K. Lundgren, and K. Runesson. Computational homogenization of diffusion in three-phase mesoscale concrete. *Computational Mechanics* **54**.2 (2014), 461–472.

[52] I. Özdemir, W. A. M. Brekelmans, and M. G. D. Geers. FE2 computational homogenization for the thermo-mechanical analysis of heterogeneous solids. *Computer Methods in Applied Mechanics and Engineering* **198**.3-4 (2008), 602–613.

[53] L. Pimienta, J. Fortin, and Y. Guéguen. Bulk modulus dispersion and attenuation in sandstones. *Geophysics* **80**.2 (2015), D111–D127.

[54] N. Pollmann, R. Jänicke, J. Renner, and H. Steeb. Experimental determination of the Skempton coefficient: Challenges and opportunities. *In review* (2019).

[55] N. Pollmann, R. Janicke, J. Renner, and H. Steeb. "Numerical Investigation of the Effective Skempton Coefficient in Porous Rock Containing Fluid-Filled Fracture Networks". *Poromechanics VI*. With permission from ASCE. 2017, pp. 1420–1427.

[56] N. Pollmann, F. Larsson, K. Runesson, and R. Jänicke. Diffuse interface modeling and Variationally Consistent Homogenization of fluid transport in fractured porous media. *In review* (2019).

[57] N. Pollmann, F. Larsson, K. Runesson, K. Lundgren, K. Zandi, and R. Jänicke. Modeling and computational homogenization of chloride diffusion in three-phase meso-scale concrete. *To be submitted for international publication* (2019).

[58] S. R. Pride and J. G. Berryman. Linear dynamics of double-porosity dual-permeability materials. I. Governing equations and acoustic attenuation. *Physical Review E* **68**.3 (2003), 036603.

[59] S. R. Pride and J. G. Berryman. Linear dynamics of double-porosity dual-permeability materials. II. Fluid transport equations. *Physical Review E* **68**.3 (2003), 036604.

[60] S. R. Pride, J. G. Berryman, and J. M. Harris. Seismic attenuation due to wave-induced flow. *Journal of Geophysical Research: Solid Earth* **109**.B1 (2004).

[61] B. Quintal, H. Steeb, M. Frehner, and S. M. Schmalholz. "Pore Fluid Effects on Seismic P-and S-wave Attenuation in Rocks with Double Porosity and Patchy Saturation". *73rd EAGE Conference and Exhibition incorporating SPE EUROPEC*. 2011.

[62] B. Quintal, J. G. Rubino, E. Caspari, and K. Holliger. A simple hydromechanical approach for simulating squirt-type flow. *Geophysics* **81**.4 (2016), D335–D344.

[63] B. Quintal, H. Steeb, M. Frehner, and S. M. Schmalholz. Quasi-static finite element modeling of seismic attenuation and dispersion due to wave-induced fluid flow in poroelastic media. *Journal of Geophysical Research: Solid Earth* **116**.B1 (2011).

[64] J. Renner and H. Steeb. Modeling of fluid transport in geothermal research. *Handbook of Geomathematics* (2015), 1443–1505.

[65] J. G. Rubino, L. Guarracino, T. M. Müller, and K. Holliger. Do seismic waves sense fracture connectivity? *Geophysical Research Letters* **40**.4 (2013), 692–696.
[66] E. H. Saenger, D. Uribe, R. Jänicke, O. Ruiz, and H. Steeb. Digital material laboratory: Wave propagation effects in open-cell aluminium foams. *International Journal of Engineering Science* **58** (2012), 115–123.
[67] C. Sandström and F. Larsson. Variationally Consistent Homogenization of Stokes Flow in Porous Media. *International Journal for Multiscale Computational Engineering* **11**.2 (2013).
[68] J. Schön. *Physical properties of rocks: A workbook*. Vol. 8. Elsevier, 2011.
[69] J. Schröder and M.-A. Keip. Two-scale homogenization of electromechanically coupled boundary value problems. *Computational Mechanics* **50**.2 (2012), 229–244.
[70] T. Schüler, R. Jänicke, and H. Steeb. Nonlinear modeling and computational homogenization of asphalt concrete on the basis of XRCT scans. *Construction and Building Materials* **109** (2016), 96–108.
[71] K. L. Scrivener, A. K. Crumbie, and P. Laugesen. The interfacial transition zone (ITZ) between cement paste and aggregate in concrete. *Interface Science* **12**.4 (2004), 411–421.
[72] H. Steeb. Ultrasound propagation in cancellous bone. *Archive of Applied Mechanics* **80**.5 (2010), 489–502.
[73] S. Teichtmeister, D. Kienle, F. Aldakheel, and M.-A. Keip. Phase field modeling of fracture in anisotropic brittle solids. *International Journal of Non-Linear Mechanics* **97** (2017), 1–21.
[74] K. Terzaghi. *Erdbaumechanik auf bodenphysikalischer Grundlage*. Deuticke, Wien, 21925.
[75] K. Terzaghi, R. B. Peck, and G. Mesri. *Soil mechanics in engineering practice*. John Wiley & Sons, 1996.
[76] C. Truesdell. "Thermodynamics of diffusion". *Rational Thermodynamics*. Springer Verlage, Berlin Heidelberg New York, 1984.
[77] A. Verruijt. *Theory and Problems of Poroelasticity*. Delft University of Technology, 2013.
[78] C. Vinci, J. Renner, and H. Steeb. On attenuation of seismic waves associated with flow in fractures. *Geophysical Research Letters* **41**.21 (2014), 7515–7523.
[79] H. F. Wang. *Theory of linear poroelasticity with applications to geomechanics and hydrogeology*. Princeton University Press, 2000.
[80] Z. M. Wang, A. K. H. Kwan, and H. C. Chan. Mesoscopic study of concrete I: Generation of random aggregate structure and finite element mesh. *Computers & structures* **70**.5 (1999), 533–544.
[81] E. Weinan. *Principles of multiscale modeling*. Cambridge University Press, 2011.
[82] J. E. White. Computed seismic speeds and attenuation in rocks with partial gas saturation. *Geophysics* **40**.2 (1975), 224–232.
[83] J. E. White, N. Mihailova, and F. Lyakhovitsky. Low-frequency seismic waves in fluid-saturated layered rocks. *The Journal of the Acoustical Society of America* **57**.S1 (1975), S30–S30.
[84] P. Wriggers and S. O. Moftah. Mesoscale models for concrete: Homogenisation and damage behaviour. *Finite Elements in Analysis and Design* **42**.7 (2006), 623–636.

[85] C. Yang and J. Su. Approximate migration coefficient of interfacial transition zone and the effect of aggregate content on the migration coefficient of mortar. *Cement and Concrete Research* **32**.10 (2002), 1559–1565.

[86] C.-C. Yang and C.-H. Liang. Determining the steady-state chloride migration coefficient of ITZ in mortar by using the accelerated chloride migration test. *Journal of the Chinese Institute of Engineers* **37**.7 (2014), 892–898.

[87] J.-j. Zheng, H. S. Wong, and N. R. Buenfeld. Assessing the influence of ITZ on the steady-state chloride diffusivity of concrete using a numerical model. *Cement and Concrete Research* **39**.9 (2009), 805–813.